A non-carboxylative route for the efficient synthesis of central metabolite malonyl-CoA and its derived products

Jian Li[1,2,7], Xin Mu[3,7], Wenyue Dong[4,7], Yun Chen[1,2], Qianjin Kang[1,2], Guang Zhao[5], Jin Hou[5], Ramon Gonzalez[6], Linquan Bai[1,2], Yan Feng[1], Chen Yang[4]✉, Tiangang Liu[1,2,3]✉ & Zaigao Tan[1,2]✉

Acetyl coenzyme A (CoA) carboxylation is the natural route for endogenous malonyl-CoA formation; however, this pathway presents slow kinetics, carbon and energy inefficiencies, tight regulations and a complicated architecture. These shortcomings limit flux towards malonyl-CoA and become a bottleneck towards the biosynthesis of malonyl-CoA-derived products (MDPs). Here, we design the non-carboxylative malonyl-CoA pathway as a non-natural route for malonyl-CoA biosynthesis, independent from acetyl-CoA. The designed pathway features enzymes such as β-alanine-pyruvate transaminase and malonyl-CoA reductase, exhibits fast kinetics and circumvents tight regulations and the architecture associated with the natural pathway. Furthermore, introducing this pathway into microbes enhances the production of MDPs, including short-chain fatty acids and representative phenol, quinone, alkene, aminoglycoside and macrolide polyketide families, such as spinosad. In summary, this malonyl-CoA formation pathway avoids intrinsic inefficiencies of the natural pathway and can serve as a versatile platform for obtaining MDPs that could be used as fuels, fine chemicals and pharmaceuticals.

Malonyl-CoA is considered a central metabolite in metabolisms. It provides the two-carbon unit for fatty acid biosynthesis and controls fatty acid oxidation by acting as the allosteric inhibitor of mitochondrial carnitine palmitoyltransferase 1 (ref. 1). At the tissue level, alterations in malonyl-CoA thus cause diseases such as obesity, diabetes, cancer and cardiovascular complications[2,3]. Malonyl-CoA acts as a cofactor for protein malonylation[2], which is a post-translational modification and is associated with diverse physiological processes, including metabolic disorders, inflammation and immune regulation[4]. In addition, malonyl-CoA serves as the building block in over 30,000 identified structures of malonyl-CoA-derived products (MDPs) including polyketides, flavonoids, coumarins and stilbenes[5]. Polyketides represent a huge class of secondary metabolites having attractive biological and pharmaceutical activities[6]. More than 10,000 polyketide structures are known so far. Of them, over 20 structures are commercial drugs (for example, erythromycin, tetracycline, avermectin and lovastatin)

[1]State Key Laboratory of Microbial Metabolism, Shanghai Jiao Tong University, Shanghai, China. [2]Department of Bioengineering, School of Life Sciences and Biotechnology, Shanghai Jiao Tong University, Shanghai, China. [3]Ministry of Education Key Laboratory of Combinatorial Biosynthesis and Drug Discovery, TaiKang Centre for Life and Medical Sciences, Zhongnan Hospital of Wuhan University, School of Pharmaceutical Sciences, Wuhan University, Wuhan, China. [4]CAS-Key Laboratory of Synthetic Biology, CAS Centre for Excellence in Molecular Plant Sciences, Chinese Academy of Sciences, Shanghai, China. [5]State Key Laboratory of Microbial Technology, Shandong University, Qingdao, China. [6]Department of Chemical, Biological and Materials Engineering, University of South Florida, Tampa, FL, USA. [7]These authors contributed equally: Jian Li, Xin Mu, Wenyue Dong. ✉e-mail: cyang@cemps.ac.cn; liutg@whu.edu.cn; ZTAN0918@sjtu.edu.cn

with annual sales of more than US$200 billion (ref. 6). Flavonoids also represent a large class of secondary metabolites with more than 15,000 structures found in nature[7]. Most of these structures have activities including antiviral, antibacterial, anti-inflammatory, anticancer and antiobesity physiological activities[8], and the global market of flavonoids may reach US$3.5 billion by 2025 (ref. 7).

Except for direct acylation of malonate, since the discovery of acetyl-CoA carboxylase (ACC) in 1958, as is well known, malonyl-CoA is produced through ACC activity in all living organisms[9]. However, ACC catalysis is a classic rate-limiting step in biochemistry. This step is associated with a series of inherent inefficiencies such as slow kinetics (specific activity being at roughly nmol min^{-1} mg^{-1}), high adenosine triphosphate (ATP) requirements (consuming one net ATP per malonyl-CoA generated), tight regulations (for example, allosteric inhibitions from long-chain fatty acyl (LCFA)-CoAs/ACPs[10]) and overexpression toxicity[11,12]. Furthermore, as acetyl-CoA is derived from pyruvate dehydrogenase (PDH) in living organisms[13], which is among the most complicated catalytic complexes known in nature (4,600–10,000 kDa)[14], PDH overexpression would bring metabolic burdens to host cells[15]. Notably, the PDH catalysis is also carbon-inefficient, releases greenhouse gas of carbon dioxide (CO_2) and leads to approximately 33% loss of carbon yield (Fig. 1a). Moreover, direct competition with multiple essential metabolic functions in cells, such as the tricarboxylic acid (TCA) cycle, amino acid biosynthesis and sterol biosynthesis for the common acetyl-CoA precursor, further limits the flux towards malonyl-CoA through the natural PDH–ACC pathway[16]. Because of these integral catalytic inefficiencies, traditional metabolic engineering efforts, such as overexpression and/or modification of the natural pathway, have a limited positive or even negative effect on malonyl-CoA and MDP synthesis[11,17,18].

Here, we show the artificial route for malonyl-CoA biosynthesis. This pathway uses 3-oxopropanoate instead of acetyl-CoA as the linking molecule, which prevents carbon loss, ATP consumption and problematic cross-talk with native metabolic networks. The feasibility of this designed pathway is demonstrated by mining suitable enzyme candidates. The non-carboxylative malonyl-CoA (NCM) pathway could substitute the natural malonyl-CoA synthesis pathway within cells. The classic regulatory inhibitions of the natural PDH–ACC catalysis are not observed during the NCM catalysis. Moreover, this proposed route causes no overexpression toxicity, but rather improves the robustness of cells to stresses. Finally, in our prototype examples, when the NCM pathway is introduced into multiple model and non-model microorganisms including *Escherichia coli*, *Streptomyces gilvosporeus* and *Saccharopolyspora spinosa*, the synthesis of various value-added MDPs is improved.

Results

Designing and implementing the NCM formation pathway

As pyruvate is the most common output of catabolic metabolism of various carbon sources[19], we designed a bridge between pyruvate and malonyl-CoA. In contrast to the natural catalytic mode of C3 (pyruvate)-C2 (acetyl-CoA)-C3 (malonyl-CoA), the design created in this study adopts a catalytic mode of C3-C3-C3 and thus bypasses the 'decarboxylation and carboxylation' reaction (Fig. 1a). Among numerous possible C3 intermediates, 3-oxopropanoate was selected as a promising candidate because it can be generated from pyruvate and converted into malonyl-CoA through a minimal number of steps (Fig. 1a). Moreover, unlike the hub metabolite acetyl-CoA, 3-oxopropanoate is not a central compound in most living cells, which thus addresses the problem of cross-talk with native metabolic networks. Specifically, the proposed pathway relies on transamination between pyruvate and β-alanine to yield 3-oxopropanoate, followed by oxidation to malonyl-CoA (Fig. 1a). In this design, no CO_2 release, carbon loss or ATP consumption occurred, indicating that the design thus dodges the inherent carbon and energy inefficiencies of the natural pathway (Fig. 1a). We termed this design the NCM formation pathway.

Next, we mined enzyme candidates for implementing the NCM formation pathway. The initial reaction of this pathway is transamination between pyruvate and β-alanine to yield 3-oxopropanoate, which is usually catalysed by β-alanine-pyruvate transaminase (EC 2.6.1.18)[20]. By combining the literature search with a molecular phylogenetic analysis (Supplementary Fig. 1), we selected five candidates including BauA from *Pseudomonas aeruginosa*[21], AptA from *Acinetobacter pittii*, CCNA_03245 from *Caulobacter vibrioides*, PydD2 from *Bacillus megaterium* and YhxA from *B. cereus* for in vitro testing (1 μM of each, Supplementary Fig. 2) (sequence alignment in Supplementary Fig. 3 and amino acid sequence in Supplementary Table 1). As expected, all these candidates exhibited desired transamination activity (Fig. 1b), with BauA (1.60 μmol min^{-1} mg^{-1}) displaying greater activity than PydD2 (0.96 μmol min^{-1} mg^{-1}), AptA (0.90 μmol min^{-1} mg^{-1}), YhxA (0.15 μmol min^{-1} mg^{-1}) and CCNA_03245 (0.13 μmol min^{-1} mg^{-1}). Thus, BauA was selected for catalysing the initial step reaction.

However, the enzyme involved in the catalysis of the second step reaction, that is, oxidation of 3-oxopropanoate to malonyl-CoA, has not been reported. Drawing inspiration from our earlier study that, for fatty acid β-oxidation, enzymes including thiolases, hydroxyacyl-CoA dehydrogenases and enoyl-CoA hydratases could be reversible and catalyse anabolic reactions[22], we put up a hypothesis. We proposed that malonyl-CoA reductases (MCRs), which originally catalyse the reductive reaction of malonyl-CoA to 3-oxopropanoate[23], might act reversibly to catalyse the desired oxidation of 3-oxopropanoate to malonyl-CoA. The Gibbs energy change indicated that this reversal is actually thermodynamically favourable ($\Delta_r G'^{\circ}$ −10.5 kcal mol^{-1}), thereby supporting our hypothesis. In addition to MCRs, succinyl-CoA reductases (SCRs), whose native catalytic substrate is succinyl-CoA, were also mined for possible promiscuity towards malonyl-CoA because succinyl-CoA has a structure analogous to that of malonyl-CoA. We then in vitro tested MCR from *Sulfurisphaera tokodaii*, the C-terminal fragment of MCR (MCR-C) from *Chloroflexus aurantiacus*[24], MCR/SCR from *Metallosphaera sedula* (Msed_0709) and two SCRs from *Pyrobaculum neutrophilum* and *Clostridium kluyveri* (SucD) (1 μM of each, Supplementary Fig. 2) (sequence alignment in Supplementary Fig. 4 and amino acid sequence in Supplementary Table 1). Among the enzymes mined, only MCR-C exhibited detectable activity (Fig. 1c). In particular, when combined with BauA, 1 μM MCR-C synthesized approximately 0.64 mM of malonyl-CoA with a maximum specific activity of 2.0 μmol min^{-1} mg^{-1} (Fig. 1c). The identity of formed malonyl-CoA was further confirmed through high-performance liquid chromatography–mass spectrometry (HPLC–MS) (Fig. 1d). This pathway presents a fast catalytic rate for malonyl-CoA formation, which was approximately 10^3-fold higher than that of the natural pathway, as evidenced by reported values of ACCs purified from *E. coli* (6 nmol min^{-1} mg^{-1})[25], *Acinetobacter baumannii* (2.3 nmol min^{-1} mg^{-1})[26], *Klebsiella pneumoniae* (19 nmol min^{-1} mg^{-1})[26], *Saccharomyces cerevisiae* ACC (23.7 nmol min^{-1} mg^{-1})[27], *Arabidopsis thaliana* (15 nmol min^{-1} mg^{-1})[28] and human (9.21 nmol min^{-1} mg^{-1})[29].

NCM pathway evades inhibitions and has a simple architecture

The natural PDH–ACC pathway is tightly regulated at multiple levels. Allosteric inhibition is among the most well-studied regulatory mechanisms: LCFA-CoAs promote fatty acid oxidation by allosterically inhibiting ACC, and this inhibition is accompanied by enzyme depolymerization[30]. An example is that 0.24 μM of palmitoyl-CoA (C16:0-CoA) led to 80% loss of ACC activity[30]. To examine whether LCFA-CoAs inhibit the NCM activity, the same amount of palmitoyl-CoA (0.24 μM) was added to the in vitro NCM system, but no decrease in malonyl-CoA formation was observed (Fig. 1e). Acetyl-CoA is a classic PDH inhibitor: 2 mM of acetyl-CoA led to nearly 70% loss of PDH activity[31]. In this study, 2 mM acetyl-CoA was added to the NCM system; however, no loss in any activity was observed (Fig. 1e). Moreover, PDH is subject to the cellular energy state, and the high ATP level inhibits PDH activity: an adenosine diphosphate (ADP)/ATP ratio of 0.1 decreases
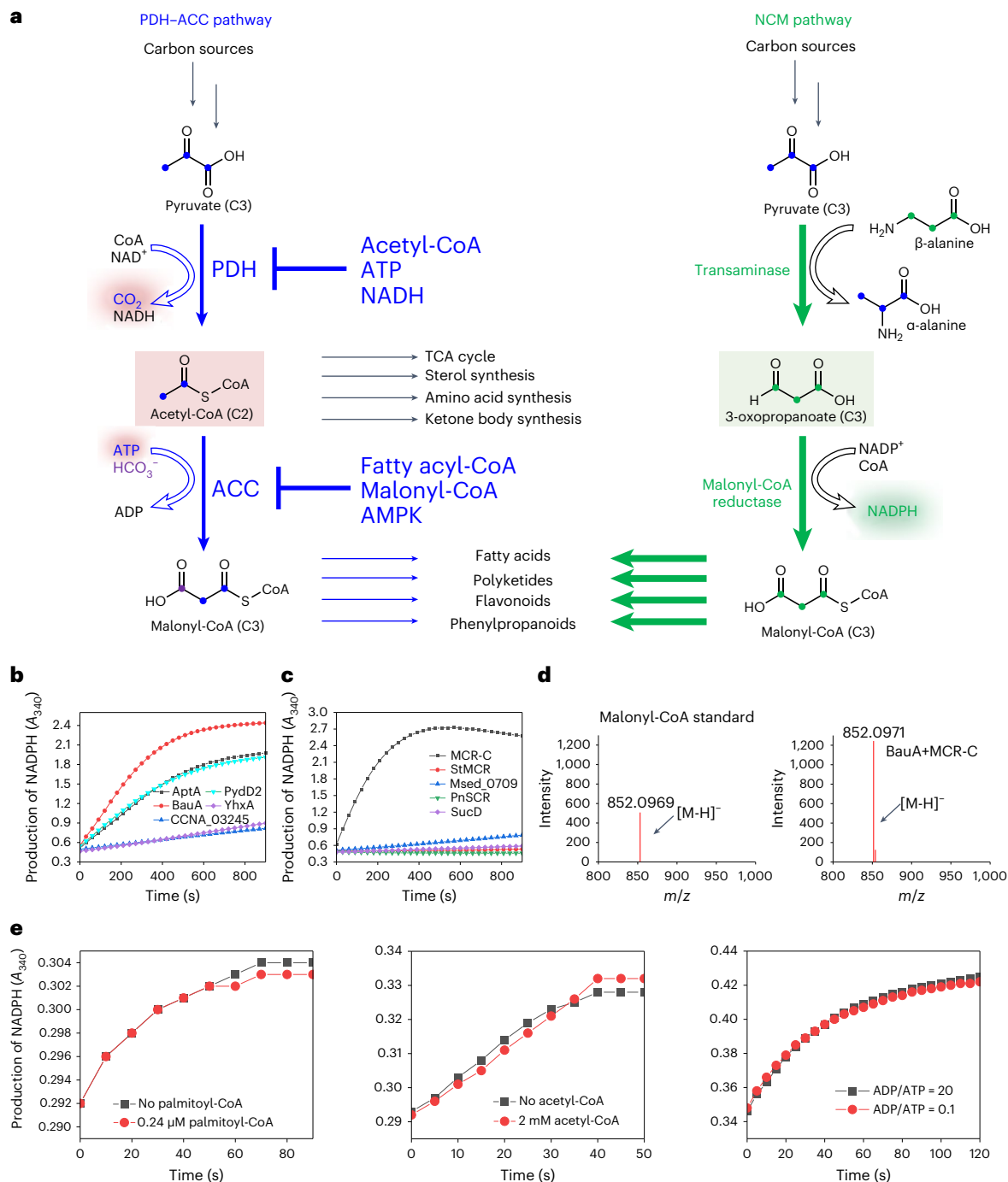
Fig. 1 | Design and implementation of an artificial pathway for malonyl-CoA biosynthesis. a, Catalysis of malonyl-CoA formation through the natural PDH–ACC pathway and non-natural NCM pathway. The natural pathway uses a 'decarboxylation and carboxylation' reaction for malonyl-CoA formation. This catalytic route releases CO_2, consumes ATP and competes for acetyl-CoA with other growth-sustaining pathways (for example, TCA cycle, sterol synthesis and amino acid synthesis). Moreover, this pathway is regulated by many allosteric inhibitors, such as fatty acyl-CoA, malonyl-CoA, free CoA, acetyl-CoA, ATP and reduced nicotinamide adenine dinucleotide (NADH), which makes malonyl-CoA formation a rate-limiting step. In contrast to the mode of C3-C2(acetyl-CoA)-C3 adopted by the natural pathway, the artificial pathway adopts a conversion mode of C3-C3(3-oxopropanoate)-C3. 3-Oxopropanoate is orthogonal to most intracellular metabolic networks, and thus addresses tight regulations from

host cells. In the artificial route, no CO_2 release, carbon loss or ATP consumption occurs. **b**, Mining β-alanine-pyruvate transaminase candidates from different sources for catalysing the initial step reaction of the NCM pathway. These candidates include BauA from *P. aeruginosa*, AptA from *A. pittii*, CCNA_03245 from *C. vibrioides*, PydD2 from *B. megaterium* and YhxA from *B. cereus*. **c**, Mining MCR candidates from different sources for catalysing the second step reaction of the NCM pathway. These candidates include MCR-C, MCR from *S. tokodaii* (StMCR), Msed_0709 and SucD. NADPH formation was monitored by the increase in absorbance at 340 nm (A_{340}). **d**, Mass spectrometry identification of the malonyl-CoA peak in the in vitro BauA + MCR-C sample through comparison with the actual standard. **e**, Classic inhibitors and/or conditions of the natural pathway do not apply to the NCM catalysis. The in vitro assays were performed according to the protocol described in the Methods section.

PDH activity to less than 10% of its maximal value[32]. By contrast, this ratio caused no decrease for the NCM system (Fig. 1e). Furthermore, to tightly regulate malonyl-CoA levels within cells, eukaryotes have

evolved the AMP-activated protein kinase that rapidly phosphorylates and inhibits ACC activity[33]. However, as NCM pathway-related enzymes originate from bacteria, this AMP-activated protein kinase-mediated

Table 1 | Comparison of natural and artificial catalytic routes for malonyl-CoA formation

	PDH–ACC pathway	NCM pathway
Product	Malonyl-CoA	
Substrate	Pyruvate	
Intermediate	Acetyl-CoA	3-Oxopropanoate
Specific activity (nmol min^{-1} mg^{-1})	2.3–23.7	2.0×10^3
Required subunit(s)/domains[a]	7	2
Size of complexes (kDa)[b]	5,000–10,000	350
Required cofactors[c]	7	3
ATP balance[d]	−1	0
Redox balance[d]	+1 NADH	+1 NADPH
Maximum CO_2 release per product[d]	+1	0
Carbon efficacy[e]	67%	100%
Number of steps	2	2
Type of chemistries involved	Decarboxylation, carboxylation	Transamination, oxidation
$\Delta_r G^{o'}$ (kcal mol^{-1})[f]	−14.3	−8.9
Competition with essential metabolisms[g]	+++	+
Tight regulation[h]	+++	+
Ease of implementation[i]	+	+++

[a] Typically, PDH consists of three subunits (E1, E2 and E3) and ACC consists of four subunits (for example, AccA, AccB, AccC and AccD of *E. coli*). By contrast, the NCM pathway consists of two subunits (BauA and MCR-C). [b] In Gram-negative bacteria, the PDH catalytic complex has an average molecular weight of approximately 4,600 kDa, and the molecular weight of this catalytic complex doubles to 8,000–10,000 kDa in gram-positive bacteria and eukaryotes. For the NCM catalysis, BauA has a molecular weight of approximately 200 kDa, with the molecular weight of MCR-C being approximately 150 kDa. [c] PDH–ACC catalysis requires seven cofactors including thiamine pyrophosphate, flavin adenine dinucleotide, CoA, nicotinamide adenine dinucleotide, lipoate, biotin and ATP. By contrast, the NCM catalysis requires three cofactors of pyridoxal phosphate, NADP$^+$ and CoA. [d] Plus (+) or minus (−) refers to generation or consumption, respectively. [e] Carbon efficacy, that is, the numbers of carbons from the substrate pyruvate in the product malonyl-CoA/the numbers of the carbons in malonyl-CoA. [f] Standard $\Delta_r G^{o'}$ of formation values are estimated using the group contribution method. [g] PDH–ACC catalysis competes with essential metabolic functions such as the TCA cycle, amino acid biosynthesis and sterol biosynthesis. By contrast, the NCM catalysis addresses problematic cross-talk with native metabolic networks. Competition with essential metabolisms is estimated with rankings of high (+++), medium (++) and low (+). [h] PDH–ACC catalysis is tightly regulated at multiple levels through steps such as allosteric inhibition, end product inhibition and ATP energy inhibition. By contrast, these inhibitions do not apply to the NCM catalysis. Tight regulation is estimated with rankings of high (+++), medium (++) and low (+). [i] Ease of implementation is estimated by factors such as enzyme availability, number of required enzymes, ability to express enzymes and complexity of enzymes with rankings of high (+++), medium (++) and low (+).

phosphorylation modification would not be effective any more. In summary, these results confirmed that the classic inhibitors and/or conditions of the natural pathway are not applicable to the artificial pathway. We also observed that the presence of a high amount of the malonyl-CoA product inhibits the activity of the NCM pathway (Supplementary Fig. 5). This can be mitigated by introducing downstream MDP biosynthesis pathways.

In gram-negative bacteria, PDH consists of 24, 24 and 12 catalytic subunits of PDH (E1), dihydrolipoyl transacetylase (E2) and dihydrolipoate dehydrogenase ([E1]$_{24}$[E2]$_{24}$[E3]$_{12}$), respectively, and has a molecular mass of approximately 4,600 kDa (ref. 34). This complex doubles to a molecular mass of 8,000–10,000 kDa in gram-positive bacteria and eukaryotes with a representative composition of [E1]$_{30}$[E2]$_{60}$[E3]$_{12}$ (ref. 35). The average mass of the ACC complex in both prokaryotes and eukaryotes is approximately 265 kDa. By contrast, BauA and MCR-C of the NCM pathway exist as a tetramer and a dimer, and have molecular masses of approximately 200 and 150 kDa, respectively (Supplementary Fig. 6). In comparison, the mass of the NCM pathway-related enzymes reduced by 93–97% (Table 1). Furthermore, the PDH–ACC catalysis requires seven cofactors, namely thiamine pyrophosphate, flavin adenine dinucleotide, CoA, nicotinamide adenine dinucleotide, lipoate, biotin and ATP. By contrast, the NCM catalysis requires three cofactors, namely pyridoxal phosphate, NADP$^+$ and CoA (Table 1). We further detected the intracellular availabilities of these cofactors in both model microorganisms (for example, *E. coli*) and non-model microorganisms (for example, *Actinomycetes*) (Extended Data Figs. 1–3), and revealed that these cofactors are relatively abundant and might not act as limiting bottlenecks for the NCM catalysis. Assuming that such simplicity will simplify the catalytic architecture for malonyl-CoA formation is reasonable.

In vivo implementation of the NCM pathway

We next explored the in vivo feasibility of the NCM pathway by using *E. coli* as a representative chassis cell. Both BauA- and MCR-C-encoding genes were cloned into the pCDFDuet-1 empty vector to generate the pCDF-*bauA-mcrC* recombinant plasmid, followed by transformation into *E. coli* MG1655 (DE3) to yield the +NCM *E. coli* strain. We detected that the intracellular malonyl-CoA content of the +NCM *E. coli* strain was 114 ± 2 nmol g^{-1} dry cell weight (DCW), which increases by 84% compared with that of the control strain (62 ± 0.7 nmol g^{-1} DCW) (Extended Data Fig. 4c).

To quantify the in vivo metabolic flux ratio between the PDH–ACC and NCM pathways in the +NCM strain, we performed isotopomer analysis by using ^{13}C-labelled glucose as the tracer. ^{13}C$_6$-glucose can produce malonyl-CoA containing two labelled carbons ($m + 2$) and three labelled carbons ($m + 3$) through the PDH–ACC pathway, or enters as the $m + 3$ isotopolog through the NCM pathway (Fig. 2a). A higher ratio of $m + 3$ was observed in the acyl-pantetheine fragment ion of malonyl-CoA (m/z 347) after NCM pathway introduction (Fig. 2b). This indicated that more glucose was converted into malonyl-CoA through the NCM catalysis. In particular, more than half glucose (mean, 57%) was converted through the NCM pathway to produce malonyl-CoA after NCM introduction, and less glucose (mean, 43%) was converted through the natural pathway (Fig. 2c). These data demonstrated the feasibility of the NCM pathway within cells.

We next determined whether the natural pathway can be substituted with the NCM pathway within cells. To this end, *accBC* genes that encode the biotin carboxyl carrier protein and biotin carboxylase of ACC in the natural pathway were initially disrupted in the *E. coli* strain (Fig. 2d,e). Cconsistent with earlier reports, *accBC* genes
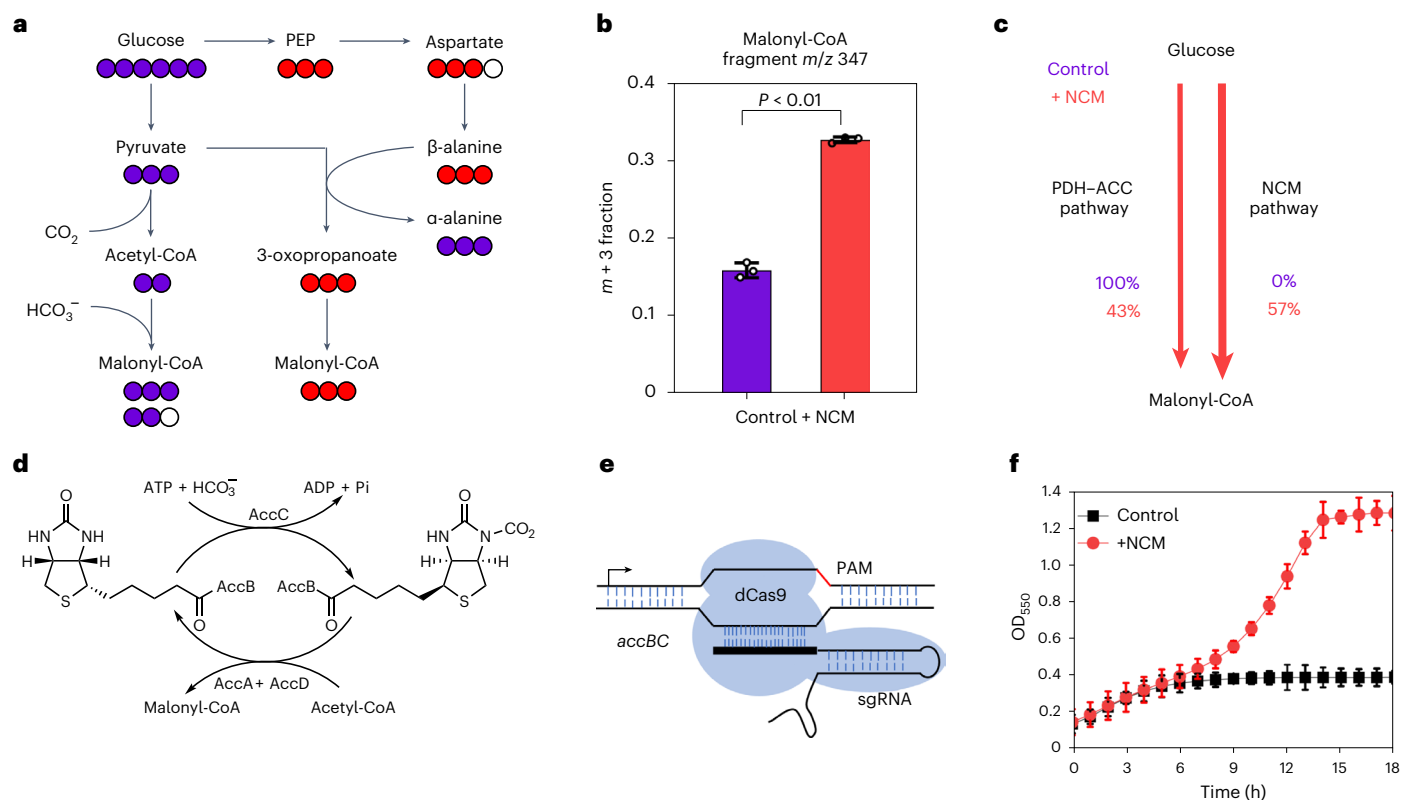
Fig. 2 | Metabolic flux after NCM pathway introduction and substituting the artificial NCM pathway for the natural pathway in *E. coli* cells. a, Schematic of [U-^{13}C] glucose-derived labelling. Purple and red circles indicate atoms arising from the PDH–ACC and NCM pathways, respectively. PEP, phosphoenolpyruvate. **b**, Fraction of the $m + 3$ isotopolog of the intracellular ^{13}C-glucose-derived malonyl-CoA fragment $m/z = 347$ in *E. coli*. $P = 9.4 \times 10^{-6}$. Data are presented as mean ± s.d. ($n = 3$ independent experiments). Statistical analysis was performed using a two-tailed Student's *t*-test. **c**, In vivo flux distribution between the PDH–

ACC and NCM catalyses in different *E. coli* strains. Data are the means of three independent experiments. **d**, Reaction mechanism of *E. coli* ACC. **e**, The CRISPRi system for transcription repression of *accBC*. PAM, protospacer adjacent motif; sgRNA, single guide RNA. **f**, The CRISPRi strategy was used for the silencing of *E. coli accBC* genes and caused growth inhibition. With the introduction of the NCM pathway, the compromised growth was restored. Data are represented as mean ± s.d. ($n = 3$ independent experiments). OD$_{550}$, optical density at 550 nm.

were not successfully deleted as they are essential for *E. coli*[36]. We next used a gene knockdown strategy, that is, CRISPR interference (CRISPRi), to repress the expression of the aforementioned genes in *E. coli* MG1655 (DE3) (Supplementary Fig. 7)[37]. When interference vectors pACYC-*dCas9* and Sg-*accBC* were introduced, evident growth inhibition was observed and the growth of the *E. coli* strain could not increase in MOPS + 2% (w/v) glucose medium because of malonyl-CoA auxotrophs (Fig. 2f). When the NCM pathway (pCDF-*bauA-mcrC*) was introduced, the *accBC* interference-induced compromise in growth was restored (Fig. 2f), which suggests that the impairment of malonyl-CoA natural biosynthesis was complemented by the NCM catalysis.

NCM pathway contributes to the robustness of cells

Previous studies have demonstrated that ACC (+ACC) overexpression often causes cellular toxicity and thus compromises cell robustness[11,12]. Next, we tested the effect of +ACC and +NCM on the growth of *E. coli* MG1655 (DE3) cells. Consistent with previous studies, the +ACC strain displayed a 50% decrease in the specific growth rate (μ, h^{-1}) from 0.50 to 0.25 h^{-1} in the absence of any inhibitors ($P < 0.01$) (Fig. 3a). In contrast to the +ACC strain, the +NCM strain exhibited a slight decline in growth under the same condition ($\mu = 0.41$ h^{-1}), suggesting that no toxicity occurred during +NCM (Fig. 3a).

The +NCM pathway allowed an improved tolerance to toxic chemicals, such as organic acids. In particular, the +NCM *E. coli* strain exhibited improved tolerance to succinate (200 mM succinate (23.6 g l^{-1})), with the cell mass (optical density at 550 nm (OD$_{550}$) = 0.60) increasing by 100% compared with that of the control *E. coli* strain (OD$_{550}$ = 0.30, $P < 0.01$) (Fig. 3a). By contrast, +ACC decreased or even abolished

bacterial growth under this challenge (OD$_{550}$ = 0.20) (Fig. 3a). This similar phenomenon was also observed when the strains were challenged with other organic acids including lactate, acetate, hexanoate, citrate, vanillic acid and levulinic acid (Fig. 3a). In addition to organic acids, the +NCM pathway allowed improved tolerance to polyketides (Fig. 3b). When the simplest polyketide (10 mM triacetic acid lactone (1.26 g l^{-1})) was present, the cell mass of the +NCM *E. coli* strain (OD$_{550}$ = 0.81) increased by 30% ($P < 0.001$) compared with that of the control *E. coli* strain (OD$_{550}$ = 0.62), which also increased by 180% ($P < 0.001$) compared with that of the +ACC *E. coli* strain (OD$_{550}$ = 0.29) (Fig. 3b). Moreover, the +NCM pathway allowed improved tolerance to adverse environmental stresses (Fig. 3c). Under higher osmotic pressure (300 mM NaCl (roughly 17.5 g l^{-1})), the cell mass of the +NCM *E. coli* strain (OD$_{550}$ = 0.76) increased by 29 and 214% ($P < 0.001$) compared with that of the control strain (OD$_{550}$ = 0.59) and the +ACC strain (OD$_{550}$ = 0.24), respectively. In the presence of a high sugar concentration (480 mM sucrose (roughly 164 g l^{-1})), the cell mass of the +NCM *E. coli* strain (OD$_{550}$ = 0.96) increased by 26 and 320% ($P < 0.001$) compared with that of the control strain (OD$_{550}$ = 0.77) and the +ACC strain (OD$_{550}$ = 0.23), respectively.

The improved tolerance probably resulted from NADPH regeneration by the NCM catalysis (Fig. 1a), as reduced nicotinamide adenine dinucleotide phosphate (NADPH) is a cofactor essential for the synthesis of the well-known glutathione antioxidant. Glutathione contributes to resist the produced reactive oxygen species when challenged with toxic inhibitors[38]. To verify this point, we further measured the intracellular NADPH/NADP$^+$ ratio in the +NCM *E. coli* strain (0.393 ± 0.005). The ratio was 59 and 69% ($P < 0.01$) higher than that in the control strain
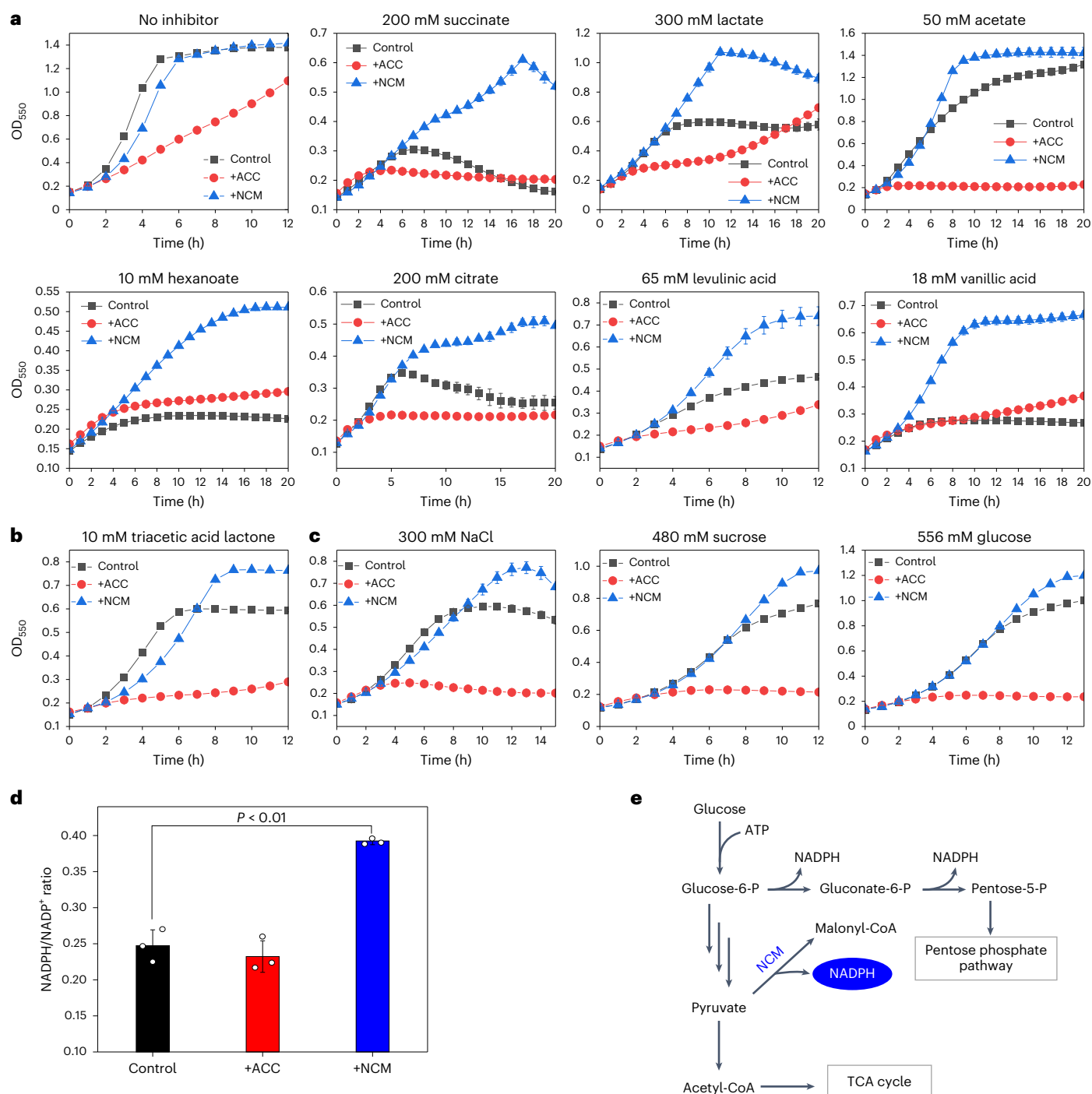
Fig. 3 | Introduction of the NCM pathway improves the robustness of cells to inhibitory chemicals and stresses. a, Introduction of the NCM pathway improved the tolerance of *E. coli* to organic acids. **b**, Introduction of the NCM pathway improved the tolerance of *E. coli* to a polyketide (triacetic acid lactone). **c**, Introduction of the NCM pathway improved the tolerance of *E. coli* to adverse environmental stresses such as high osmotic pressure (NaCl) and high sugars (sucrose and glucose). Growth curves were recorded in the MOPS + 2% (w/v)

glucose medium containing different concentrations of inhibitors added to a clear-bottom 96-well plate at 37 °C with an initial pH of 7.0. **d**, Introduction of the NCM pathway led to higher intracellular levels of NADPH. $P = 0.0037$. All data are represented as mean ± s.d. ($n = 3$ independent experiments). Statistical analysis was performed using a two-tailed Student's t-test. **e**, The NCM pathway acts as an additional source for NADPH regeneration in the central carbon metabolism.

(0.247 ± 0.022) and +ACC strain (0.232 ± 0.022), respectively (Fig. 3d). In central carbon metabolism, the oxidative branch of the pentose phosphate pathway and isocitrate dehydrogenase of the TCA cycle are mainly the canonical sources of NADPH regeneration[39]. Our work adds the NCM catalysis as an additional source for NADPH regeneration (Fig. 3e).

Harnessing the NCM pathway for MDP synthesis in vivo
We then investigated the effect of the NCM pathway on the in vivo synthesis of diverse MDPs, with the initial analysis conducted in fatty acid production. Octanoic acid (C8) is a representative short-chain fatty acid and is used in fuel, food preservation, health promotion and disease control[40]. A type II fatty acid synthesis system produces
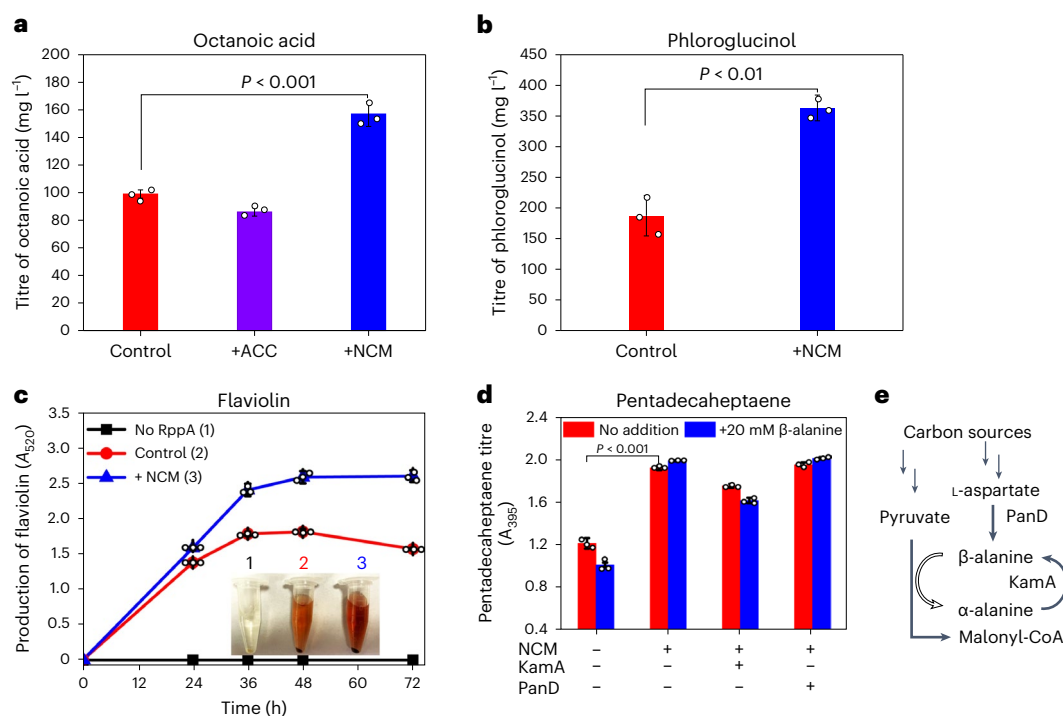
Fig. 4 | Introduction of the NCM pathway into the model organism *E. coli* improved MDP production. a, Introduction of the NCM pathway (pCDF-*bauA*-*mcr-C*) increased short-chain fatty acid (octanoic acid, C8) production. Both *E. coli* strains with the pCum-*TE10* plasmid carrying the thioesterase 10 (TE10) specific for C8 release were cultivated in the M9 + 2% (w/v) glucose medium in shake flasks at 30 °C and an initial pH of 7.0 for 72 h. *P* = 0.00048. **b**, Introduction of the NCM pathway increased phloroglucinol production. Both *E. coli* strains with the pCum-*phlD* plasmid were cultivated in the M9 + 2% (w/v) glucose medium in shake flasks at 37 °C and an initial pH of 7.0 for 48 h. *P* = 0.0015. **c**, Introduction of the NCM pathway increased flaviolin production. Both *E. coli* strains with the pCum-*rppA* plasmid carrying the *RppA* gene were cultivated in the M9 + 2% (w/v) glucose medium in shake flasks at 37 °C and initial pH 7.0 for 72 h. The inset shows the supernatant of strains 1, 2 and 3. The

supernate of strain 1 is transparent, because there is not synthetase (RppA) of red-coloured flaviolin. The strain 3 with NCM pathway and flaviolin synthetase produced more flaviolin than strain 2, which only contains flaviolin synthetase, and the supernate of strain 3 is therefore redder than strain 2. **d**, Introduction of the NCM pathway increased pentadecaheptaene production. Both *E. coli* strains with PKS I SgcE with cognate thioesterase SgcE10 were cultivated in LB medium in shake flasks at 37 °C and an initial pH of 7.0 for 72 h. Both supplemented 20 mM β-alanine (one substrate of NCM pathway) in the medium and overexpressed enzymes involved β-alanine synthesis or regeneration, no obvious increase was observed in the pentadecaheptaene titre. *P* = 2.21 × 10⁻⁵. **e**, Synthetic or regeneration pathway for β-alanine. All data are represented as mean ± s.d. (*n* = 3 independent experiments). Statistical analysis was performed using a two-tailed Student's *t*-test.

octanoyl-ACP by condensing three malonyl-CoA molecules and one acetyl-CoA molecule[41] (Extended Data Fig. 5a). For free C8 production, TE10 thioesterase from *Anaerococcus tetradius*, which primarily hydrolyses octanoyl-ACP, was used[41]. We codon-optimized and synthesized the *TE10* gene and introduced the pCum-*TE10* plasmid into both control and +NCM *E. coli* strains. Although the final biomass was not influenced (Extended Data Fig. 6a), the +NCM *E. coli* strain with pCum-*TE10* produced 157 ± 9 mg l⁻¹ of C8 (Fig. 4a), which was 58% higher than that produced by the control strain (99 ± 3 mg l⁻¹) (*P* < 0.02), whereas the overexpression of *Corynebacterium glutamicum* ACC decreased the C8 titre to 86 ± 3 mg l⁻¹ (Fig. 4a).

In addition to fatty acids, we applied the NCM pathway for synthesizing other MDP types. Phloroglucinol, a representative member of the phenol polyketide family, has been used to alleviate pain and synthesize many bioactive molecules such as hyperforin, adhyperforin and rhotomensones[42]. PhlD, a type III polyketide synthase (PKS III), synthesized phloroglucinol by condensing three malonyl-CoA molecules (Extended Data Fig. 5b). The *phlD* gene was obtained from *P. protegens*, and the pCum-*phlD* plasmid was introduced into both control and +NCM *E. coli* strains. The results revealed that the +NCM strain with pCum-*phlD* produced almost 363 ± 21 mg l⁻¹ of phloroglucinol (Fig. 4b), which was 94% higher than that produced by the control strain (187 ± 33 mg l⁻¹) (*P* < 0.01). The biomass of the +NCM strain (OD₅₅₀ = 2.91 ± 0.01) was roughly 14% higher than that of the control strain (OD₅₅₀ = 2.56 ± 0.09) (Extended Data Fig. 6b).

In addition to phenol polyketides, quinone polyketides are another class of appealing MDPs, as illustrated by flaviolin, that serve as the moiety for the synthesis of a class of polyketide-isoprenoid hybrid compounds including naphterpin, napyradiomycin A and marinone with antioxidative, antitumour and anticancer activities[43]. The potential of the NCM platform was next tested for the synthesis of flaviolin, which is more structurally complex than the aforementioned phloroglucinol. In particular, flaviolin is synthesized by PKS III (1,3,6,8-tetrahydroxynaphthalene synthase, RppA) by condensing five malonyl-CoA molecules[44,45] (Extended Data Fig. 5c). We codon-optimized and synthesized the *rppA* gene from *S. griseus*[44] and introduced the pCum-*rppA* plasmid into both control and +NCM *E. coli* strains. According to the results, the flaviolin titre in the +NCM strain with pCum-*rppA* (A₅₂₀ = 2.57 ± 0.09) was almost 43% higher than that in the control strain (A₅₂₀ = 1.81 ± 0.04) (*P* < 0.01) (Fig. 4c). The biomass of the +NCM *E. coli* strain (OD₅₅₀ = 5.7 ± 0.07) was 19% higher than that of the control strain (OD₅₅₀ = 4.79 ± 0.14) (Extended Data Fig. 6c).

We tested whether the NCM pathway can be applied to MDPs synthesized by PKS I/IIs, in addition to their production by PKS III products. To this end, we synthesized the representative alkene pentadecaheptaene, which is the key intermediate in the biosynthesis of enediyne (a well-known anticancer antibiotic), as well as a biofuel with high energy content[46]. A PKS I SgcE with a cognate thioesterase SgcE10 synthesizes pentadecaheptaene by condensing seven malonyl-CoA molecules and one acetyl-CoA molecule[47] (Extended
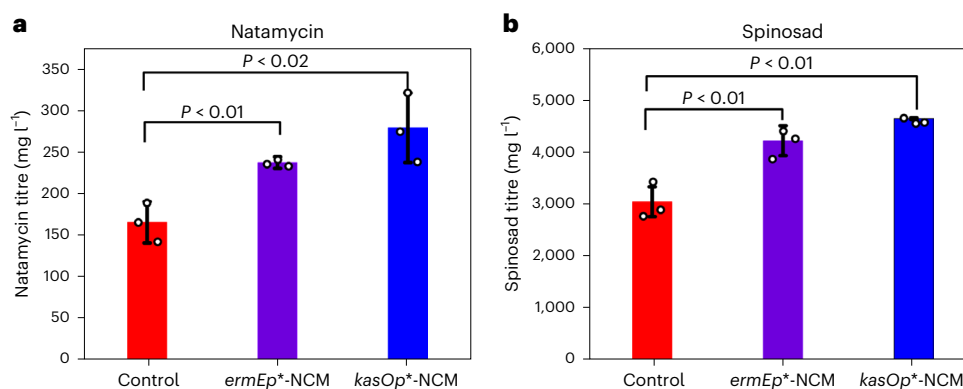
Fig. 5 | Introduction of the NCM pathway into non-model microorganisms improved MDP production. a, Introduction of the NCM pathway increased natamycin production in *S. gilvosporeus*. A moderate-activity *ermE*p* promoter and a high-activity *kasO*p* promoter were used to regulate the expression of NCM pathway-related enzymes and increased natamycin titres by 42 and 67%, respectively. *P* value is 0.0088 between control and *ermE*p*-NCM and the *P* value is 0.016 between control and *kasO*p*-NCM. **b**, Introduction of the NCM pathway

increased spinosyn production in *S. spinosa*. The moderate-activity *ermE*p* and high-activity *kasO*p* promoters were used to regulate the expression of NCM pathway-related enzymes and increased spinosyn titres by 38 and 52%, respectively. The *P* value is 0.0074 between control and *ermE*p*-NCM, and *P* is 0.0006 between control and *kasO*p*-NCM. All data are represented as mean ± s.d. (*n* = 3 independent experiments). Statistical analysis was performed using a two-tailed Student's *t*-test.

Data Fig. 5d). When the NCM pathway was introduced into an earlier developed pentadecaheptaene-producing *E. coli* strain pQL1 (ref. 46), a 59% increase was observed in the pentadecaheptaene titre (A_{395} from $1.21 ± 0.05$ to $1.92 ± 0.02$, $P < 0.02$) (Fig. 4d). The biomass of the +NCM *E. coli* strain ($OD_{550} = 1.60 ± 0.03$) was 19% higher than that of the control strain ($OD_{550} = 1.35 ± 0.02$) (Extended Data Fig. 6d).

Because β-alanine is required by the NCM catalysis as a precursor for transamination, we wondered whether the availability of intracellular β-alanine might act as a limiting bottleneck for the NCM pathway. To this end, we improved the β-alanine supply in the +NCM *E. coli* strain and examined its effect on pentadecaheptaene production. First, 20 mM β-alanine was supplemented in the medium. No obvious increase was observed in the pentadecaheptaene titre (A_{395} from $1.92 ± 0.02$ to $1.98 ± 0.01$) (Fig. 4d). In addition to exogenous supply systems, two endogenous β-alanine supply systems were developed. First, a β-alanine recycling system that converts generated α-alanine back to β-alanine was developed, and the corresponding enzyme of alanine 2,3-aminomutase (KamA) from *B. subtilis*[48,49] was thus introduced into the +NCM *E. coli* strain (Fig. 4e). Yet, KamA introduction slightly decreased pentadecaheptaene titres to A_{395} of $1.75 ± 0.02$ (no addition of β-alanine) and $1.61 ± 0.03$ (+20 mM β-alanine) (Fig. 4d). Second, the key enzyme aspartate 1-decarboxylase of *E. coli* (PanD)[50] that converts L-aspartate to β-alanine in the +NCM *E. coli* strain was overexpressed (Fig. 4e). However, this strategy maintained the pentadecaheptaene levels at A_{395} of $1.95 ± 0.02$ (no addition of β-alanine) and $2.01 ± 0.01$ (+20 mM β-alanine) (Fig. 4d). Thus, in the representative chassis *E. coli* cells, the intracellular β-alanine level was sufficient for supporting the NCM catalysis. We further detected the availability of intracellular β-alanine in other microorganisms, such as *Actinomycetes* (Extended Data Fig. 7). Results revealed that the intracellular levels of β-alanine in these microorganisms are abundant for supporting NCM catalysis. Consistent with this conclusion, β-alanine is the only naturally occurring β-type amino acid and can be synthesized by diverse living organisms including bacteria, fungi and plants[51].

Broad application of the NCM pathway

To investigate whether the NCM catalysis can be used in other microorganisms beyond the aforementioned model *E. coli*, we introduced the pathway into non-model microorganisms. *S. gilvosporeus* is a high G+C gram-positive bacteria that belongs to *Actinomycetes*[52]. Moreover, it is a native producer of natamycin (pimaricin), a representative aminoglycoside antibiotic, which is the only antifungal agent recognized

by the US Food and Drug Administration[53]. Natamycin production is initiated by a large PKS I, which uses 12 malonyl-CoA molecules and one methylmalonyl-CoA molecule as substrates (Extended Data Fig. 8a). The *S. gilvosporeus* starter strain produced $168 ± 25$ mg l^{-1} natamycin in shake flasks (Fig. 5a). First, the NCM pathway was introduced and the expression levels of genes related to this pathway were regulated using a moderate-activity promoter *ermE*p* (ref. 54). A 42% increase in the natamycin titre to $240 ± 7$ mg l^{-1} was observed ($P < 0.01$) (Fig. 5a, biomass data in Extended Data Fig. 6e), which was consistent with the increase in the intracellular malonyl-CoA content (Extended Data Fig. 4a). Then, a high-activity promoter *kasO*p* (ref. 54) was used to further increase the expression of NCM pathway enzymes, and the natamycin titre further increased by 67% to $282 ± 42$ mg l^{-1} in the shake flasks ($P = 0.016$) (Fig. 5a, biomass data in Extended Data Fig. 6e).

In addition to *E. coli* and *S. gilvosporeus*, we assessed the applicability of the NCM pathway in other types of cell for synthesizing other MDP types. *S. spinosa* is a gram-positive, non-motile, filamentous bacteria and the native producer for spinosad (a mixture of spinosyns A and D). Spinosad represents a broad-spectrum macrolide insecticide[55]. Spinosad production is initiated by a PKS I, which uses nine malonyl-CoA molecules, one propionyl-CoA molecule and one methylmalonyl-CoA molecule as substrates (Extended Data Fig. 8b). The *S. spinosa* WHU1107 starter strain produced approximately $3,050 ± 284$ mg l^{-1} spinosad (Fig. 5b). The expression of NCM pathway enzymes by using the moderate-activity promoter *ermE*p* in *S. spinosa* WHU1107 resulted in a 38% increase in the spinosad titre to $4,212 ± 285$ mg l^{-1} ($P = 0.015$) (Fig. 5b, see biomass data in Extended Data Fig. 6f), which was also consistent with the increase in intracellular the malonyl-CoA content (Extended Data Fig. 4b). Moreover, a high-activity promoter *kasO*p* further increased the spinosad titre by 52% to $4,637 ± 18$ mg l^{-1} in shake flasks ($P = 0.0014$) (Fig. 5b, biomass data and malonyl-CoA content in Extended Data Figs. 6f and 4b, respectively). This is a very high spinosad titre in native or engineered microbes under cultivation conditions. All these results have further demonstrated the broad applicability of the NCM pathway across multiple microorganisms for efficient MDP synthesis.

Discussion

The synthesis of the building block malonyl-CoA, catalysed by the natural PDH–ACC pathway, is considered a limiting step for achieving high titres of fatty acids, polyketides, flavonoids and other MDPs[56]. This is expected given the primary supporting role of the natural PDH–ACC

pathway in cell growth and survival during natural evolution rather than serving as a dedicated route for high-efficient MDP synthesis[57]. The randomicity and constraints of natural evolution should not restrict the ideal means of producing the central metabolite malonyl-CoA, but be rationally designed. Instead of working within the confinements of the natural pathway, artificial malonyl-CoA formation pathways that circumvent these inherent inefficiencies must be designed for the efficient synthesis of diverse MDPs.

We here demonstrated the design, prototyping, implementation and application of a synthetic pathway for malonyl-CoA formation. This pathway targeted 3-oxopropanoate as a catalytic linking intermediate between pyruvate and malonyl-CoA. We had sought to further optimize the NCM catalysis by constructing multienzyme complexes to prevent potential intermediate leakage, thereby further improving malonyl-CoA and MDP production. In particular, a pair of short peptide tags (RIAD and RIDD)[58] to create scaffold-free enzyme assemblies to achieve these goals (Extended Data Fig. 9). However, although different assemblies were made, for example, RIAD-BauA/RIDD-MCR-C and RIDD-BauA/RIAD-MCR-C, a limited increase was achieved when compared with +NCM without assemblies (Extended Data Fig. 9). This suggested no leakage of the intermediate 3-oxopropanoate during NCM catalysis, which was also consistent with the in vitro data that purified BauA and MCR-C enzymes have comparable activities (1.60 versus 2.0 μmol min^{-1} mg^{-1}). Moreover, although our design initially targeted 3-oxopropanoate as a key linking intermediate, in principle, any other C3 compound can potentially serve as the catalytic linking intermediate for malonyl-CoA biosynthesis.

The NCM pathway evades many stoichiometric and regulatory constraints associated with the PDH–ACC catalysis[31,32] (Table 1). We also compared the NCM pathway with other pathways, for the production of MDPs in terms of carbon and energy efficiency (Supplementary Table 2). The effectiveness of the NCM catalysis was demonstrated by improving the synthesis of representative MDPs of fatty acids (octanoic acid), phenols (phloroglucinol), quinones (flaviolin), alkenes (pentadecaheptaene), aminoglycosides (natamycin) and macrolides (spinosad). Although the NCM catalysis was mainly implemented here in representative bacteria including E. coli, S. gilvosporeus and S. spinosa, further application of this pathway in other bacteria and eukaryotes[59] is feasible for accessing the vast range of MDPs. In this study, most MDP titres were obtained in minimal salt media and/or under shake flask cultivation. Further optimization of fermentation conditions[44] would contribute to higher MDP titres. Moreover, because of its role in malonyl-CoA synthesis, ACC has so far become a primary target for treating metabolic diseases, including obesity, diabetes, hypertension and cancer[60]. In future, the NCM pathway has a potential to act as the therapeutic target against these metabolic diseases.

Methods

Plasmid construction

All plasmids used in this study are listed in Supplementary Table 3. For mining β-alanine-pyruvate transaminase candidates, genes encoding BauA from P. aeruginosa, AptA from A. pittii, CCNA_03245 from C. vibrioides, PydD2 from B. megaterium and YhxA from B. cereus were synthesized by Sangon Biotech with codon optimization. For mining MCR candidates, genes encoding MCRs from C. aurantiacus (MCR-C) and S. tokodaii, SucD and Msed_0709 were synthesized by Sangon Biotech with codon optimization.

To construct the NCM pathway plasmid, both bauA and mcrC genes were inserted into a pCDFDuet-1 plasmid (Novagen) by using the Seamless Cloning Kit (Beyotime) to yield the pCDF-bauA-mcrC plasmid. To construct the two plasmids with different endogenous β-alanine supply systems, the kamA gene that encodes B. subtilis alanine 2,3-aminomutase was further inserted into the pCDF-bauA-mcrC plasmid to yield the pCDF-bauA-mcrC-kamA plasmid. Similarly, the panD gene from E. coli that encodes aspartate 1-decarboxylase was inserted

into the pCDF-bauA-mcrC plasmid to yield the pCDF-bauA-mcrC-panD plasmid. To construct pACYC-dCas9, an already developed pCF plasmid expressing TesA' and dCas9 (ref. 37) was used as the template and the TesA' was removed by using the Seamless Cloning Kit (Beyotime). To construct Sg-accBC, a Sg-0 plasmid developed earlier[37] was used as template, with the N20 sequence changing to GTTGCGGGTATAAAGCAGAT by using the Seamless Cloning Kit (Beyotime).

To construct the pCum-TE10 plasmid, the gene encoding thioesterase (TE10) from Anaerococcus tetradius was inserted into the pCum empty plasmid and under the control of cumate-inducible T5 promoter by using the Seamless Cloning Kit (Beyotime, Shanghai, China). Similarly, to construct pCum-phlD and pCum-rppA plasmids, the gene encoding phloroglucinol synthase from P. protegens and the gene encoding RppA from S. griseus were inserted into the pCum empty plasmid, respectively.

Overexpression of the NCM pathway in S. gilvosporeus and S. spinosa is based on the plasmid pSET152, which can be integrated into the genomic DNA through site-specific recombination[61]. Primer pairs kasOp-F/R and SPL42-F/R were used to amplify promoters kasOp* and SPL42 from pLH10 and pLH2, respectively[62]. Primers bauA-F/R and mcrC-F/R were used to amplify bauA and mcrC from pCDF-bauA-mcrC (see sequence of the primers Supplementary Table 4). The amplified fragments were joined through overlap extension polymerase chain reaction (PCR) conducted using primers kasOp-F/bauA-R and SPL42-F/mcrC-R. Two joined fragments were cloned into pSET152 by using the One Step Cloning Kit (Yeasen), yielding the recombinant pSET152-kasOp*-bauA-SPL42-mcrC plasmid. The plasmid pSET152-ermEp*-bauA-ermEp*-mcrC was obtained in the same way.

Strain construction

All constructed strains are listed in Supplementary Table 3. For production of chemicals in E. coli, the MG1655 (DE3) strain was used as the host strain. When necessary, antibiotics were added at the final concentrations of: ampicillin (100 μg ml^{-1}), spectinomycin (50 μg ml^{-1}), kanamycin (50 μg ml^{-1}) and chloramphenicol (17 μg ml^{-1}).

For production of natamycin in S. gilvosporeus, the NCM pathway was transferred into S. gilvosporeus by biparental conjugation. The plasmid donor E. coli ET12567 (pUZ8002) containing recombinant plasmid was cultured to the logarithmic phase. After washing twice in Luria-Bertani (LB) medium, cells were suspended in a small volume of LB. The recipient S. gilvosporeus J1-002 was cultivated on the soya flour mannitol (SFM) agar plate at 30 °C for 7 days, and the spores were suspended in 0.05 M TES(N-(Tris(hydroxymethyl)methyl))-2-aminoethanesulfonic acid) buffer (pH 8.0) and incubated at 50 °C for 10 min to active germination. Then, an equal volume of double-strength germination medium (0.1 g l^{-1} Difco Yeast Extract, 0.1 g l^{-1} Difco Casmino acid and 0.01 M CaCl$_2$) was added and the mixture was incubated at 37 °C for 2–3 h with shaking at 220 rpm. The germinated spores were collected by centrifugation and suspended in TSE buffer. The E. coli cells and S. gilvosporeus cells were mixed and spread on the SFM agar plate containing 10 mM MgCl$_2$. The conjugation plate was cultured for 14–16 h at 30 °C and then the surface of the plate was covered in 2 ml of sterile water with 1.25 mg of apramycin and 1.25 mg of trimethoprim. After culturing for 7–9 days at 30 °C, transconjugants were selected and verified by PCR analysis.

For production of spinosad in S. gilvosporeus, the NCM pathway was transferred into S. spinosa by triparental conjugation. The plasmid donors E. coli DH10b (recombinant plasmid), E. coli ET12567 (pUB307) and the recipient S. spinosa WHU1107 were cultured to the logarithmic phase. After washing twice in LB medium, these strains were mixed together and spread on the ABB13 agar plate (5 g l^{-1} soluble starch, 5 g l^{-1} Difco Soytone, 2.1 g l^{-1} 4-Morpholinepropanesulfonic acid, 3 g l^{-1} CaCO$_3$, 0.046 g l^{-1} FeSO$_4$, 0.01 g l^{-1} VBI, pH 7.2) containing 10 mM MgCl$_2$. The conjugation plate was cultured for 20–22 h at 28 °C and then the surface of the plate was covered in 2 ml of sterile water with 675 μg

apramycin and 1.25 mg trimethoprim. After culturing for 8–10 days at 28 °C, transconjugants were selected and verified by PCR analysis.

In vitro assays

E. coli BL21 (DE3) was used as the host strain for expression of His-tagged proteins. BL21 (DE3) strains harbouring pCDF-*bauA* or pCDF-*mcrC* plasmid were grown at 37 °C in 50 ml of fresh LB medium with spectinomycin at the initial OD$_{550}$ of roughly 0.1. When OD$_{550}$ of the culture increased to 0.4–0.8, isopropyl-β-D-thiogalactoside (IPTG) was added at a final concentration of 0.1 mM for induction. After 4–6 h of induction at 37 °C, cells were gathered by centrifugation. The cell pellet was washed twice using ddH$_2$O and resuspended in the lysis buffer (50 mM Na$_2$HPO$_4$, 300 mM NaCl, 10 mM imidazole, pH 8.0) and subjected to sonication using a Sonifier SFX250 (Branson). Following centrifugation (10,000g, 4 °C, 15 min), the soluble protein in the supernatant was purified by using a His-tag Protein Purification Kit (Beyotime). The final protein concentrations were determined by using the Bradford Protein Assay Kit (Beyotime).

For mining β-alanine-pyruvate transaminase, the in vitro assays were performed in a 200 μl total reaction volume containing 100 mM Tris-HCl buffer (pH 7.8), 3 mM EDTA, 2 mM MgCl$_2$, 5 mM pyruvate, 5 mM β-alanine, 5 mM NADP$^+$, 5 mM CoA, 1 μM purified β-alanine-pyruvate transaminase and 10 μM purified MCR-C. The increase in absorbance at 340 nm (NADPH formation) was monitored.

For mining MCR, the in vitro assays were performed in a 200 μl total reaction volume containing 100 mM Tris-HCl buffer (pH 7.8), 3 mM EDTA, 2 mM MgCl$_2$, 5 mM pyruvate, 5 mM β-alanine, 5 mM NADP$^+$, 5 mM CoA, 10 μM purified BauA and 1 μM purified MCR. The increase in absorbance at 340 nm (NADPH formation) was monitored.

The in vitro assays for NCM pathway were performed in a 200 μl total reaction volume containing 100 mM Tris-HCl buffer (pH 7.8), 3 mM EDTA, 2 mM MgCl$_2$, 5 mM pyruvate, 5 mM β-alanine, 5 mM NADP$^+$, 5 mM CoA, 10 μM purified BauA and 10 μM purified MCR-C. For measuring the specific activity of NCM pathway for malonyl-CoA formation, the increase in absorbance at 340 nm (NADPH formation) was monitored. The identity of formed malonyl-CoA was further confirmed through HPLC–MS. Methanol (100 μl) was added to the in vitro malonyl-CoA samples, centrifuged at 11,000g for 5 min to remove the protein pellets, filtered and then subjected to LC–MS analysis using an Agilent 1200 HPLC system and Bruker MicroToF electrospray ionization LC–MS system. The column was an Eclipse Plus C18 column (3.0 × 150 mm, 3.5 μm, Agilent). An HPLC column was used to separate malonyl-CoA and other components of the in vitro assay at 40 °C with 10 mM ammonium acetate in water (A) and 10 mM ammonium acetate in acetonitrile (B) as mobile phases. The elution procedure was used as follows: 0.4 ml min^{-1} flow rate, 0–5 min, 90% A and 10% B to 80% A and 20% B; 6–20 min, 80% A and 20% B to 100% B; 21–25 min, 100% B to 90% A and 10% B; 26–27 min, 90% A and 10% B.

To examine the potential inhibitory effects of LCFA-CoA, the in vitro assays were performed in a 200 μl total reaction volume containing 50 mM Tris-HCl buffer (pH 7.5), 1 mM DTT, 10 mM MgCl$_2$, 0.13 mM pyruvate, 0.13 mM β-alanine, 0.13 mM NADP$^+$, 0.13 mM CoA, 24 uM pamityl-CoA, 0.1 μM purified BauA and 0.1 μM purified MCR-C. For measuring the specific activity of the NCM pathway for malonyl-CoA production, the increase in absorbance at 340 nm (NADPH formation) was monitored.

To examine the potential inhibitory effects of acetyl-CoA, the in vitro assays were performed in a 200 μl total reaction volume containing 100 mM Tricien buffer (pH 8), 3 mM DTT, 5 mM MgCl$_2$, 1 mM pyruvate, 1 mM β-alanine, 1 mM NADP$^+$, 0.1 mM CoA, 2 mM acetyl-CoA, 1 μM purified BauA and 1 μM purified MCR-C. For measuring the specific activity of the NCM pathway for malonyl-CoA production, the increase in absorbance at 340 nm (NADPH formation) was monitored.

To examine the potential inhibitory effects of ADP/ATP, the in vitro assays were performed in a 200 μl total reaction volume

containing 40 mM potassium HEPES (pH 7.1), 0.8 mM DTT, 0.8 mM MgCl$_2$, 1 mM pyruvate, 1 mM β-alanine, 0.5 mM NADP$^+$, 0.5 mM CoA, (ATP + ADP = 3.75 mM, ADP/ATP = 20 and 0.1), 1 μM purified BauA and 1 μM purified MCR-C. For measuring the specific activity of the NCM pathway for malonyl-CoA production, the increase in absorbance at 340 nm (NADPH formation) was monitored.

Isotope labelling experiments

E. coli cells were exponentially grown in M9 containing 10 g l^{-1} glucose. The cells were collected by centrifugation and transferred into the media containing 10 g l^{-1} of a mixture of 50% (wt/wt) [U-^{13}C] glucose and 50% unlabelled glucose. After 45 min of cultivation, cells corresponding to a biomass of 20 ml of optical density of roughly 0.5 were collected through centrifugation, and metabolites were extracted with 1 ml of −80 °C 80% methanol[63]. After incubation at −20 °C for 20 min, the samples were centrifuged and the supernatant was collected.

Amino acids were analysed by gas chromatography–MS (GC–MS) (GC7890-MS7200QTOF, Agilent). The dried cell extracts were derivatized with N-methyl-N-($tert$-butyldimethylsilyl)trifluoroacetamide (Sigma) at 70 °C for 30 min. After filtration, 2 μl of samples were injected into the GC–MS system with an DB-5HT column (30 × 0.25 mm, 0.1 μm). The mass spectrometer was operated in the electron impact mode at 70 eV.

Acyl-CoAs were analysed by ultrahigh performance liquid chromatography (Acquity, Waters) coupled to a Q Exactive hybrid quadrupole-orbitrap mass spectrometer (Thermo Fisher) as described before[64]. The injection volume was 10 μl. Tandem MS (MS/MS) spectra for acetyl-CoA and malonyl-CoA were acquired on the same mass spectrometer operated in positive ionization mode. Precursor ions of the metabolites were targeted as [M + H]$^+$ with a window size of 2 m/z. Fragment-ion spectra were recorded at a 17,500 resolution.

Metabolic flux analysis

Mass isotopomer distributions of intact and fragmented metabolites were determined from measured peak areas of the mass spectra and corrected for naturally occurring stable isotopes as described before[63]. All calculations were performed with MATLAB v.7.8.0 (Mathworks). To quantify the relative contribution of PDH–ACC pathway versus NCM pathway in the formation of malonyl-CoA, the labelling pattern of acyl-CoAs and amino acids were measured. Because β-alanine cannot be separated with α-alanine, labelling of the C2–C4 fragment of aspartate was used (Asp316 of GC derivatization), which is decarboxylased to form β-alanine. The MS/MS-measured mass isotopomer distributions of the acyl-pantetheine fragment ion of acetyl-CoA (ACA303) and malonyl-CoA (MCA347) were used to rule out the disturbance of the adenosine part. The flux distribution between PDH–ACC pathway and NCM pathway was obtained:

$$L_{MCA347} = f L_{ACA303} L_{CO2} + (1 - f) L_{Asp316}$$

where f is the flux ratio of PDH–ACC pathway, L_{MCA347} is the ^{13}C labelling degree of the MCA347 fragment, L_{ACA303} is the ^{13}C labelling degree of the ACA303 fragment, L_{CO2} is the ^{13}C labelling degree of CO$_2$ and L_{Asp316} is the ^{13}C labelling degree of the Asp316 fragment.

CRISPRi assays

E. coli MG1655 (DE3) harbours pACYC-*dCas9*, and the Sg-*accBC* (N20 sequence for *accBC*: CCACTGATTTCCGCTGCTGC) for CRISPRi assay was performed in 200 μl of the MOPS + 2% (wt/v) glucose minimal medium in a clear-bottom 96-well plate at 37 °C at an initial pH of 7.0, and 0.3 mM IPTG.

Fermentation medium and conditions

For octanoic acid fermentation, the overnight seed culture was inoculated into 50 ml of the M9 + 2.0% (wt/v) glucose medium in 250-ml

shake flasks with an initial OD_{550} = 0.1. As the OD_{550} reached roughly 0.6, 0.1 mM IPTG and 0.25 mM cumate were added. Cultures were grown at 30 °C and 220 rpm for 72 h. Octanoic acid production was quantified using an Agilent 7890 gas chromatograph equipped with an Agilent 5975 mass spectrometer (GC–MS) after extraction. Briefly, 1 ml of culture was mixed with 125 μl of 10% (wt/v) sodium chloride and 125 μl of acetic acid. Then, 20 μl of 1 mg ml^{-1} heptanoic acid (C7:0) was added to the mixture, followed by 500 μl of ethyl acetate. The mixture was vortexed for 30 s and centrifuged at 16,000g for 10 min. Then, 250 μl of the top organic phase was transferred to a separate glass tube followed by the addition of 2.25 ml of ethanol:hydrochloric acid (30:1 v/v). After incubation at 55 °C for 1 h, 1.25 ml of double-distilled water (ddH_2O) and 1.25 ml of hexane were added, vortexed and centrifuged at 2,000g for 2 min. The top hexane layer was then transferred and analysed through GC–MS. The initial temperature maintained for GC–MS analysis was at 50 °C for 2 min, which was ramped to 200 °C at 25 °C min^{-1}, held for 1 min, raised to 315 °C at 25 °C min^{-1} and held for 2 min. Helium was used as a carrier gas and the flow rate set was 1 ml min^{-1} through a DB-5MS separation column (30 m, 0.25 mm ID, 0.25 μm, Agilent).

For phloroglucinol and flaviolin fermentations, the overnight seed culture was inoculated into 50 ml of the M9 + 2.0% (wt/v) glucose medium in 250-ml shake flasks with an initial OD_{550} of 0.1. As the OD_{550} reached roughly 0.6, 0.1 mM IPTG and 0.25 mM cumate were added. Cultures were grown at 37 °C and 220 rpm for 72 h. The phloroglucinol concentration was analysed using the Agilent 1200 HPLC system and Bruker MicroToF (ToF, time of flight) electrospray ionization LC–MS System. The column used was Eclipse Plus C18 column (3.0 × 150 mm, 3.5 μm, Agilent). The flaviolin concentration was measured by evaluating A_{520} of the culture supernatant[65].

For pentadecaheptaene fermentation, the overnight culture was inoculated into 50 ml of LB medium in 250-ml shake flasks (and 20 mM β-alanine was added or not) with an initial OD_{550} of 0.1. As the OD_{550} reached roughly 0.6, 0.1 mM IPTG was added. Cultures were grown at 37 °C and at 220 rpm for 72 h. The pentadecaheptaene concentration was measured by A_{395} of culture supernatant[5].

For natamycin fermentation, *S. gilvosporeus* and its derivatives were cultivated on the SFM agar plate at 30 °C for 10 days. Then 1 cm^2 agar block with spores was grown in the seed medium (15 g l^{-1} glucose, 12 g l^{-1} yeast powder, 10 g l^{-1} NaCl, 0.2 g l^{-1} defoaming agent, pH 7.0) at 28 °C with 200 rpm for 24 h. According to 5% inoculation amount, the seed fermentation cultures was transferred to fermentation medium (40 g l^{-1} glucose, 30 g l^{-1} Difco Soytone, 8 g l^{-1} yeast powder, 0.001 g l^{-1} biotin, pH 7.1), at 200 rpm for 5 days at 28 °C. Natamycin was extracted from the fermentation cultures (1 ml) by mixing with 9 ml methanol, vortexed for 3 min, and the cell wall was destroyed by ultrasonication, after which suspensions were centrifuged at 8,000g for 15 min. The supernatant was filtered using a 0.22 μm syringe filter and injected into the C18-reversed phase HPLC column at 30 °C using isocratic elution with methanol:water (6:4) at a flow rate of 0.7 ml min^{-1} and detection at 303 nm.

For spinosad fermentation, *S. spinosa* WHU1107 and its derivatives were cultivated on 019 agar plate (5 g l^{-1} glucose, 3 g l^{-1} yeast extract, 10 g l^{-1} N-Z amine type A, 20 g l^{-1} agar, pH 7.0) at 28 °C for 7 days. Then a 1 cm^2 agar block with spores was grown in the seed medium (10 g l^{-1} glucose, 10 g l^{-1} yeast extract, 2 g l^{-1} N-Z amine type A, 25 g l^{-1} cottonseed meal, 20 g l^{-1} corn starch, 2 g l^{-1} MgSO$_4$·7H$_2$O, 1 g l^{-1} ammonium sulfate, pH 7.0) at 28 °C with 250 rpm for 96 h. According to the 1% inoculation amount, seed fermentation cultures were transferred to the secondary seed medium (same to the seed medium), 250 rpm for 60 h at 28 °C. According to the 5% inoculation amount, the secondary seed fermentation cultures were transferred to fermentation medium (80 g l^{-1} glucose, 20 g l^{-1} cottonseed meal, 10 g l^{-1} protein powder, 5 g l^{-1} yeast powder, 4 g l^{-1} sodium citrate, 2 g l^{-1} di-potassium hydrogen phosphate, 3 g l^{-1} CaCO$_3$, 2 g l^{-1} ammonium sulfate, 50 g l^{-1} rapeseed oil, pH 7.0), 250 rpm for 12 days at 28 °C. Spinosad was extracted from

the fermentation cultures (1 ml) by mixing with 4 ml of ethanol, vortexed for 20 min and centrifuged at 8,000g for 15 min. The supernatant was filtered using a 0.22 μm syringe filter and injected into the C18-reversed phase HPLC column at 25 °C using isocratic elution with methanol:acetonitrile:water containing 0.05% ammonium acetate (45:45:10) at a flow rate of 1 ml min^{-1} and detection at 250 nm (ref. 55).

Tolerance assays

E. coli tolerance assays were performed in 200 μl of the MOPS + 2% (wt/v) glucose minimal medium[1] in a clear-bottom 96-well plate at 37 °C at an initial pH of 7.0 and 0.1 mM IPTG. To calculate the specific growth rate (h^{-1}), the equation $OD_{550,t} = OD_{550,0}e^{\mu t}$ to the exponential growth phase was used.

NADPH and NADP$^+$ assays

The *E. coli*, *S. gilvosporeus* and *S. spinosa*, cells were collected through centrifugation at 6,000g for 10 min at 4 °C at the logarithmic growth phase and the stationary phase of fermentation.

The NADPH and NADP$^+$ contents were measured by using the NADP$^+$/NADPH Assay Kit (Beyotime), and the NADPH/NADP$^+$ ratio was thus calculated.

Measurements of β-alanine and malonyl-CoA using the ELISA kit

The *E. coli*, *S. gilvosporeus* and *S. spinosa*, cells were collected through centrifugation at 6,000g for 10 min at 4 °C at the logarithmic growth phase and the stationary phase of fermentation.

The cells were then resuspended in 2 ml of ice-cold PBS buffer, and the cell wall was destroyed through ultrasonication. The suspensions were then centrifuged at 8,000g for 10 min at 4 °C. The β-alanine and malonyl-CoA concentrations in the supernatant were measured using a β-alanine enzyme-linked immunosorbent assay (ELISA) kit (Fankew, Shanghai Kexing Trading Co., Ltd) and a malonyl-CoA ELISA kit (Fankew, Shanghai Kexing Trading Co., Ltd) for microbes according to the manufacturer's instructions, respectively.

Extraction and analysis of PLP and CoA by LC–MS

Cell suspensions of the *S. gilvosporeus* and *S. spinosa* strains cultured in 5 ml of fermentation medium for the logarithmic growth phase and the stationary phase were removed through centrifugation at 6,000g for 10 min at 4 °C. Then 200 μl of pickling glass beads (0.5 mm) and 1 ml of extraction solvent (methanol:acetonitrile:H$_2$O = 2:2:1) were added to the cells. The cells were vortexed for 1 min, ice bathed for 1 min and cycled five times to destroy the cell wall. The suspensions were then centrifuged at 8,000g for 10 min at 4 °C, and the supernatants were transferred into a separate tube and lyophilized. The samples were resuspended in 200 μl of 50% methanol, vortexed for 1 min and sonicated in a water bath for 2 min. The samples were centrifuged at 12,000g for 10 min at 4 °C and the supernatants were used for pyridoxal 5'-phosphate (PLP) and CoA analyses using the HPLC high-resolution mass spectrometer (HPLC-HRMS, Ulti-Mate 3000 system, Dinoex, coupled with a Q Exactive Orbitrap mass analyser, Thermo Fisher). The method of PLP and CoA analyses has been described in ref. 54.

The *E. coli* cells were collected through centrifugation at 6,000g for 10 min at 4 °C. Metabolites were extracted with 1 ml of 80% methanol at −80 °C. After incubation at −20 °C for 20 min, the samples were centrifuged and the supernatant was collected. The PLP concentration was determined through HPLC. The chromatographic conditions were as follows: the chromatographic column was Zorbax Eclipse Plus C18 (4.6 × 250 mm, 5 mm). The mobile phase was acetonitrile: water (30:70, v/v). The pH of the mobile phase was adjusted to 6.0 with potassium dihydrogen phosphate buffer (20 mM). The ultraviolet detection wavelength was 255 nm. The column temperature was 30 °C, the injection volume was 10 μl and the flow rate of the mobile phase was 0.8 ml min^{-1}. The CoA concentration was determined through LC–MS/MS[63]

Statistics and reproducibility

No statistical method was used to predetermine sample size. No data were excluded from the analyses. The experiments were not randomized. The investigators were not blinded to allocation during experiments and outcome assessment. The two-tailed t-test method was used to analyse the statistical significance of all data in this study and $P < 0.05$ is deemed statistically significant.

Reporting summary

Further information on research design is available in the Nature Portfolio Reporting Summary linked to this article.

Data availability

All the data generated in this study are available within the main text and the Supplementary Information file. Source data are provided with this paper. Data are also available from the corresponding author upon request.

References

1. Bowman, C. E. & Wolfgang, M. J. Role of the malonyl-CoA synthetase ACSF3 in mitochondrial metabolism. *Adv. Biol. Regul.* **71**, 34–40 (2019).
2. Wang, Y. et al. Acetyl-CoA carboxylases and diseases. *Front. Oncol.* **12**, 836058 (2022).
3. Folmes, C. D. & Lopaschuk, G. D. Role of malonyl-CoA in heart disease and the hypothalamic control of obesity. *Cardiovasc. Res.* **73**, 278–287 (2007).
4. Zou, L. et al. Lysine malonylation and its links to metabolism and diseases. *Aging Dis.* **14**, 84–98 (2023).
5. Yang, Y. et al. Regulating malonyl-CoA metabolism via synthetic antisense RNAs for enhanced biosynthesis of natural products. *Metab. Eng.* **29**, 217–226 (2015).
6. Chan, Y. A. et al. Biosynthesis of polyketide synthase extender units. *Nat. Prod. Rep.* **26**, 90–114 (2009).
7. Sajid, M. et al. Synthetic biology towards improved flavonoid pharmacokinetics. *Biomolecules* **11**, 754 (2021).
8. Safe, S. et al. Flavonoids: structure-function and mechanisms of action and opportunities for drug development. *Toxicol. Res.* **37**, 147–162 (2021).
9. Wakil, S. J. A malonic acid derivative as an intermediate in fatty acid synthesis. *J. Am. Chem. Soc.* **80**, 6465–6465 (1958).
10. Shi, S. et al. Improving production of malonyl coenzyme A-derived metabolites by abolishing Snf1-dependent regulation of Acc1. *mBio* **5**, e01130–14 (2014).
11. Johnson, A. O. et al. Design and application of genetically-encoded malonyl-CoA biosensors for metabolic engineering of microbial cell factories. *Metab. Eng.* **44**, 253–264 (2017).
12. Davis, M. S., Solbiati, J. & Cronan, J. E. Overproduction of acetyl-CoA carboxylase activity increases the rate of fatty acid biosynthesis in *Escherichia coli*. *J. Biol. Chem.* **275**, 28593–28598 (2000).
13. Kozak, B. U. et al. Engineering acetyl coenzyme A supply: functional expression of a bacterial pyruvate dehydrogenase complex in the cytosol of *Saccharomyces cerevisiae*. *mBio* **5**, e01696–14 (2014).
14. Skerlova, J. et al. Structure of the native pyruvate dehydrogenase complex reveals the mechanism of substrate insertion. *Nat. Commun.* **12**, 5277 (2021).
15. Atherton, H. J. et al. Role of pyruvate dehydrogenase inhibition in the development of hypertrophy in the hyperthyroid rat heart: a combined magnetic resonance imaging and hyperpolarized magnetic resonance spectroscopy study. *Circulation* **123**, 2552–2561 (2011).
16. Milke, L. & Marienhagen, J. Engineering intracellular malonyl-CoA availability in microbial hosts and its impact on polyketide and fatty acid synthesis. *Appl. Microbiol. Biotechnol.* **104**, 6057–6065 (2020).
17. Leonard, E. et al. Engineering central metabolic pathways for high-level flavonoid production in *Escherichia coli*. *Appl. Environ. Microbiol.* **73**, 3877–3886 (2007).
18. Wu, J. et al. Enhancing flavonoid production by systematically tuning the central metabolic pathways based on a CRISPR interference system in *Escherichia coli*. *Sci. Rep.* **5**, 13477 (2015).
19. Francois, J. M., Alkim, C. & Morin, N. Engineering microbial pathways for production of bio-based chemicals from lignocellulosic sugars: current status and perspectives. *Biotechnol. Biofuels* **13**, 118 (2020).
20. Stinson, R. A. & Spencer, M. S. Beta alanine aminotransferase (s) from a plant source. *Biochem. Biophys. Res. Commun.* **34**, 120–127 (1969).
21. Wilding, M. et al. A beta-alanine catabolism pathway containing a highly promiscuous omega-transaminase in the 12-aminododecanate-degrading *Pseudomonas* sp. strain AAC. *Appl. Environ. Microbiol.* **82**, 3846–3856 (2016).
22. Dellomonaco, C. et al. Engineered reversal of the bβ-oxidation cycle for the synthesis of fuels and chemicals. *Nature* **476**, 355–359 (2011).
23. Liu, C. et al. Dissection of malonyl-coenzyme A reductase of *Chloroflexus aurantiacus* results in enzyme activity improvement. *PLoS ONE* **8**, e75554 (2013).
24. Liu, C. et al. Functional balance between enzymes in malonyl-CoA pathway for 3-hydroxypropionate biosynthesis. *Metab. Eng.* **34**, 104–111 (2016).
25. Davis, M. S. & Cronan, J. E. Jr Inhibition of *Escherichia coli* acetyl coenzyme A carboxylase by acyl-acyl carrier protein. *J. Bacteriol.* **183**, 1499–1503 (2001).
26. Alves, J. et al. Cloning, expression, and enzymatic activity of *Acinetobacter baumannii* and *Klebsiella pneumoniae* acetyl-coenzyme A carboxylases. *Anal. Biochem.* **417**, 103–111 (2011).
27. Mishina, M., Roggenkamp, R. & Schweizer, E. Yeast mutants defective in acetyl-coenzyme A carboxylase and biotin: apocarboxylase ligase. *Eur. J. Biochem.* **111**, 79–87 (1980).
28. Sun, J. D. et al. Biochemical and molecular biological characterization of CAC2, the *Arabidopsis thaliana* gene coding for the biotin carboxylase subunit of the plastidic acetyl-coenzyme A carboxylase. *Plant Physiol.* **115**, 1371–1383 (1997).
29. Kim, K. W. et al. Expression, purification, and characterization of human acetyl-CoA carboxylase 2. *Protein Expr. Purif.* **53**, 16–23 (2007).
30. Yeh, L. A., Song, C. S. & Kim, K. H. Coenzyme A activation of acetyl-CoA carboxylase. *J. Biol. Chem.* **256**, 2289–2296 (1981).
31. Qi, Q. et al. Pyruvate dehydrogenase complex and acetyl-CoA carboxylase in pea root plastids: their characterization and role in modulating glycolytic carbon flow to fatty acid biosynthesis. *J. Exp. Bot.* **47**, 1889–1896 (1996).
32. Hansford, R. G. Studies on the effects of coenzyme A-SH:acetyl coenzyme A, nicotinamide adenine dinucleotide:reduced nicotinamide adenine dinucleotide, and adenosine diphosphate:adenosine triphosphate ratios on the interconversion of active and inactive pyruvate dehydrogenase in isolated rat heart mitochondria. *J. Biol. Chem.* **251**, 5483–5489 (1976).
33. Herzig, S. & Shaw, R. J. AMPK: guardian of metabolism and mitochondrial homeostasis. *Nat. Rev. Mol. Cell Biol.* **19**, 121–135 (2018).
34. Sumegi, B. et al. Electron microscopic study on the size of pyruvate dehydrogenase complex *in situ*. *Eur. J. Biochem.* **169**, 223–230 (1987).

35. Walter, C., Marada, A. & Meisinger, C. Monitoring checkpoints of metabolism and protein biogenesis in mitochondria by Phos-tag technology. *J. Proteom.* **252**, 104430 (2022).

36. Baba, T. et al. Construction of *Escherichia coli* K-12 in-frame, single-gene knockout mutants: the Keio collection. *Mol. Syst. Biol.* **2**, 0008 (2006). 2006.

37. Fang, L. et al. Genome-scale target identification in *Escherichia coli* for high-titer production of free fatty acids. *Nat. Commun.* **12**, 4976 (2021).

38. Olin-Sandoval, V. et al. Lysine harvesting is an antioxidant strategy and triggers underground polyamine metabolism. *Nature* **572**, 249–253 (2019).

39. Spaans, S. K. et al. NADPH-generating systems in bacteria and archaea. *Front. Microbiol.* **6**, 742 (2015).

40. Tan, Z. et al. Engineering of *E. coli* inherent fatty acid biosynthesis capacity to increase octanoic acid production. *Biotechnol. Biofuels* **11**, 87 (2018).

41. Tan, Z. et al. Membrane engineering via trans unsaturated fatty acids production improves *Escherichia coli* robustness and production of biorenewables. *Metab. Eng.* **35**, 105–113 (2016).

42. Rizzo, P., Altschmied, L., Ravindran, B. M., Rutten, T. & D'Auria, J. C. The biochemical and genetic basis for the biosynthesis of bioactive compounds in *Hypericum perforatum* L., one of the largest medicinal crops in Europe. *Genes* **11**, 1210 (2020).

43. Kawasaki, T. et al. Biosynthesis of a natural polyketide-isoprenoid hybrid compound, furaquinocin A: identification and heterologous expression of the gene cluster. *J. Bacteriol.* **188**, 1236–1244 (2006).

44. Tan, Z., Clomburg, J. M. & Gonzalez, R. Synthetic pathway for the production of olivetolic acid in *Escherichia coli*. *ACS Synth. Biol.* **7**, 1886–1896 (2018).

45. Yan, D. et al. Repurposing type III polyketide synthase as a malonyl-CoA biosensor for metabolic engineering in bacteria. *Proc. Natl Acad. Sci. USA* **115**, 9835–9844 (2018).

46. Liu, Q. et al. Engineering an iterative polyketide pathway in *Escherichia coli* results in single-form alkene and alkane overproduction. *Metab. Eng.* **28**, 82–90 (2015).

47. Zhang, J. et al. A phosphopantetheinylating polyketide synthase producing a linear polyene to initiate enediyne antitumor antibiotic biosynthesis. *Proc. Natl Acad. Sci. USA* **105**, 1460–1465 (2008).

48. Chen, D., Ruzicka, F. J. & Frey, P. A. A novel lysine 2,3-aminomutase encoded by the *yodO* gene of *bacillus subtilis*: characterization and the observation of organic radical intermediates. *Biochem. J.* **348**, 539–549 (2000).

49. Jessen, H. J. et al. Alanine 2, 3 aminomutases. US Patent Application 11/658,795 (2009).

50. Lacmata, S. T. et al. Enhanced poly(3-hydroxypropionate) production via beta-alanine pathway in recombinant *Escherichia coli*. *PLoS ONE* **12**, e0173150 (2017).

51. Wang, L. et al. Advances in biotechnological production of beta-alanine. *World J. Microbiol. Biotechnol.* **37**, 79 (2021).

52. Zong, G. et al. Complete genome sequence of the high-natamycin-producing strain *Streptomyces gilvosporeus* F607. *Genome Announc.* **6**, e01402–e01417 (2018).

53. Wang, Y. M. et al. Iteratively improving natamycin production in *Streptomyces gilvosporeus* by a large operon-reporter based strategy. *Metab. Eng.* **38**, 418–426 (2016).

54. Wang, X., Deng, Z. & Liu, T. Marker-free system using ribosomal promoters enhanced xylose/glucose isomerase production in *Streptomyces rubiginosus*. *Biotechnol. J.* **14**, e1900114 (2019).

55. An, Z. et al. Increasing the heterologous production of spinosad in *Streptomyces albus* J1074 by regulating biosynthesis of its polyketide skeleton. *Synth. Syst. Biotechnol.* **6**, 292–301 (2021).

56. Choi, J. W. & Da Silva, N. A. Improving polyketide and fatty acid synthesis by engineering of the yeast acetyl-CoA carboxylase. *J. Biotechnol.* **187**, 56–59 (2014).

57. Tan, Z. et al. Designing artificial pathways for improving chemical production. *Biotechnol. Adv.* **64**, 108119 (2023).

58. Kang, W. et al. Modular enzyme assembly for enhanced cascade biocatalysis and metabolic flux. *Nat. Commun.* **10**, 4248 (2019).

59. Crawford, J. M. & Townsend, C. A. New insights into the formation of fungal aromatic polyketides. *Nat. Rev. Microbiol.* **8**, 879–889 (2010).

60. Chen, L. et al. Acetyl-CoA carboxylase (ACC) as a therapeutic target for metabolic syndrome and recent developments in ACC1/2 inhibitors. *Expert Opin. Inv. Drugs* **28**, 917–930 (2019).

61. Bierman, M. et al. Plasmid cloning vectors for the conjugal transfer of DNA from *Escherichia coli* to *Streptomyces* spp. *Gene* **116**, 43–49 (1992).

62. Liu, Q. et al. Development of *Streptomyces* sp. FR-008 as an emerging chassis. *Synth. Syst. Biotechnol.* **1**, 207–214 (2016).

63. Yuan, J. et al. Kinetic flux profiling for quantitation of cellular metabolic fluxes. *Nat. Protoc.* **3**, 1328–1340 (2008).

64. Dong, W. et al. Mycobacterial fatty acid catabolism is repressed by FdmR to sustain lipogenesis and virulence. *Proc. Natl Acad. Sci. USA* **118**, e2019305118 (2021).

65. Krauser, S., Kiefer, P. & Heinzle, E. Multienzyme whole-cell in situ biocatalysis for the production of flaviolin in permeabilized cells of *Escherichia coli*. *Chem. Cat. Chem.* **4**, 786–788 (2012).

Author contributions

Z.T., T.L. and C.Y. designed the research. J.L., X.M. and Y.C. performed the in vitro and in vivo analysis of NCM pathway. W.D. and C.Y. performed the metabolic flux analysis. Q.K., G.Z. and J.H. constructed the plasmids. Z.T., T.L., C.Y., J.L., X.M., W.D., Y.C., Q.K., G.Z., J.H., R.G., L.B. and Y.F. analysed the data. Z.T., T.L., C.Y. and R.G. wrote the paper.

Competing interests

The authors declare no competing interests.

Additional information

Extended data is available for this paper at https://doi.org/10.1038/s41929-023-01103-2.

Supplementary information The online version contains supplementary material available at https://doi.org/10.1038/s41929-023-01103-2.

Correspondence and requests for materials should be addressed to Chen Yang, Tiangang Liu or Zaigao Tan.

Peer review information *Nature Catalysis* thanks Yaping Xue, Dongsoo Yang and the other, anonymous, reviewer(s) for their contribution to the peer review of this work.
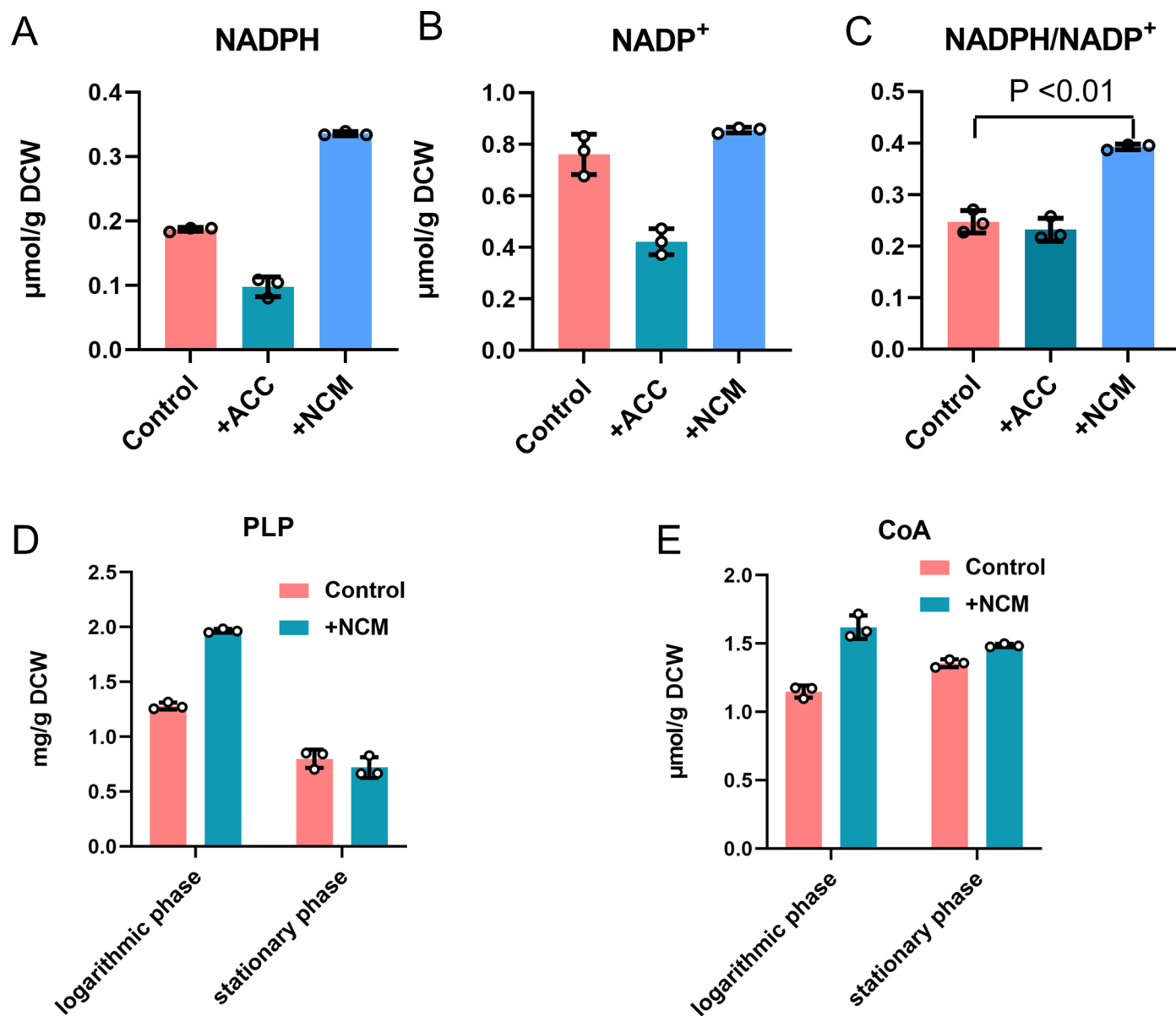
**Reprints and permissions information** is available at www.nature.com/reprints.

Extended Data Fig. 1 | The intracellular contents of NCM pathway cofactors in *E. coli*. a, The intracellular concentration of NADPH in *E. coli*. **b**, The intracellular concentration of NADP⁺ in *E. coli*. **c**, The NADPH/NADP⁺ ratio in *E. coli*. P = 0.0037. **d**, The intracellular concentrations of PLP in *E. coli* at logarithmic growth phase and stationary phase. **e**, The intracellular concentrations of CoA in *E. coli* at logarithmic growth phase and stationary phase. All data were represented as mean ± SD (n = 3 independent experiments). Statistical analysis was performed using two-tailed Student's *t*-test.
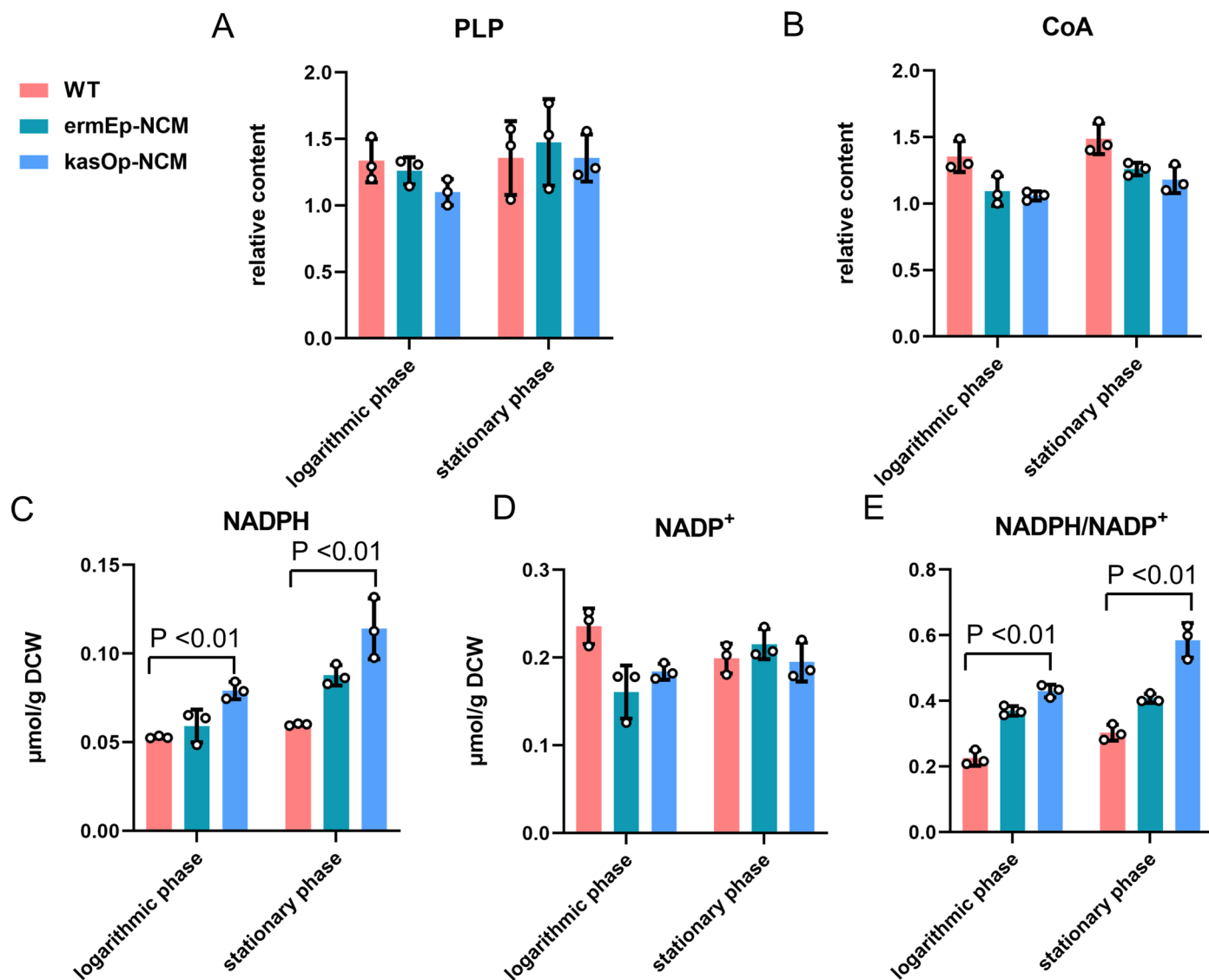
Extended Data Fig. 2 | The intracellular contents of PLP, CoA, NADPH, NADP⁺ and NADPH/NADP⁺ ratio in *Streptomyces gilvosporeus*. a, The relative content of PLP in *Streptomyces gilvosporeus* at logarithmic growth phase and stationary phase. **b**, The relative content of CoA in *Streptomyces gilvosporeus* at logarithmic growth phase and stationary phase. (The relative content: we set the sample with the smallest peak area to 1, and the remaining samples are converted according to the peak area ratio). **c**, The content of NADPH per dry cell weight in *Streptomyces gilvosporeus* at logarithmic growth phase and stationary phase. P value is 0.0007 at logarithmic phase and is 0.0055 at stationary phase. **d**, The content of NADP⁺ per dry cell weight in *Streptomyces gilvosporeus* at logarithmic growth phase and stationary phase. **e**, The molar ratio of NADPH/NADP⁺ in *Streptomyces gilvosporeus* at logarithmic growth phase and stationary phase. P value is 0.0003 at logarithmic phase and is 0.0011 at stationary phase. All data were represented as mean ± SD (n = 3 independent experiments). Statistical analysis was performed using two-tailed Student's *t*-test.
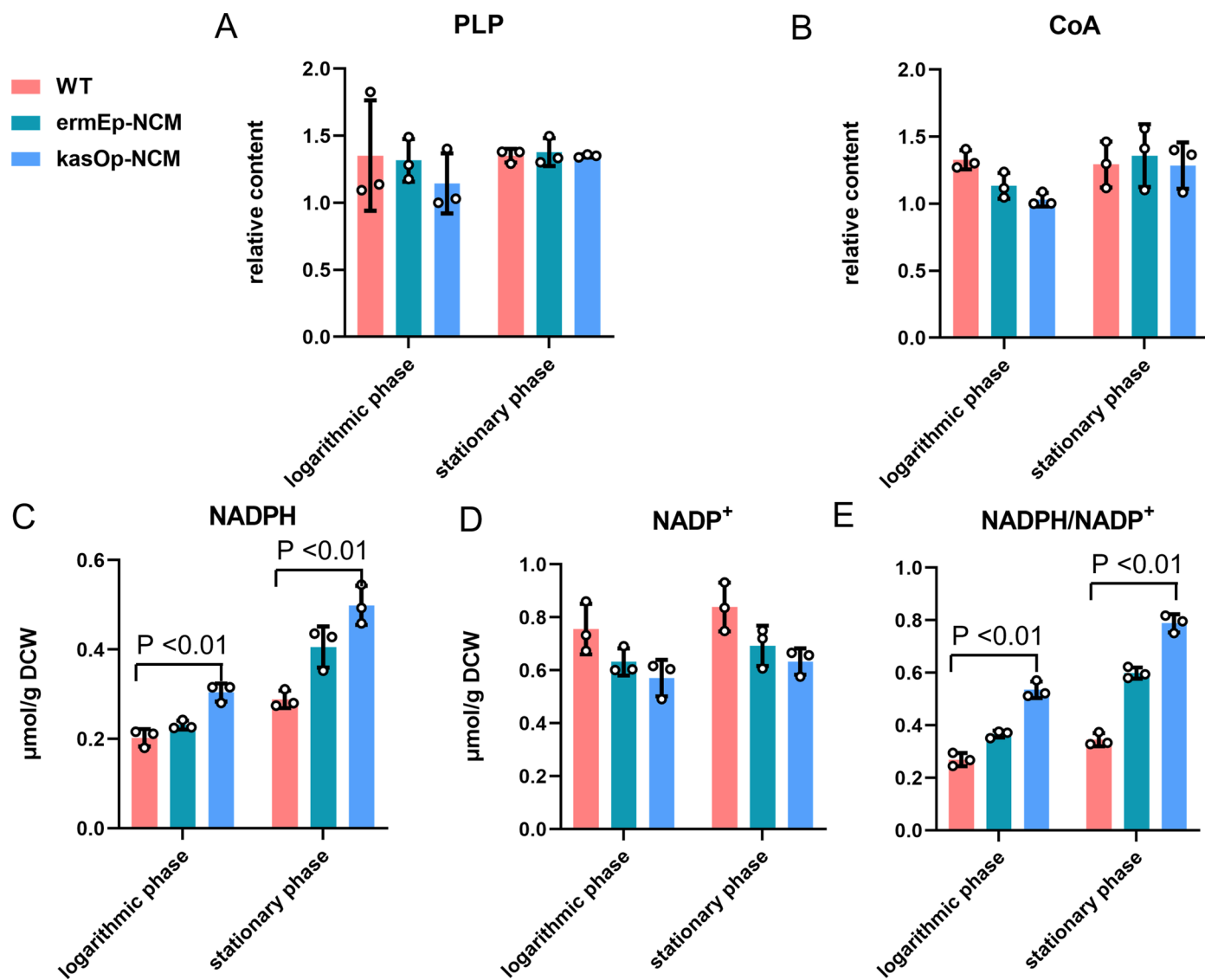
Extended Data Fig. 3 | The intracellular contents of PLP, CoA, NADPH, NADP+ and NADPH/NADP+ ratio in *Saccharopolyspora spinosa*. a, The relative content of PLP in *Saccharopolyspora spinosa* at logarithmic growth phase and stationary phase. **b**, The relative content of CoA in *Saccharopolyspora spinosa* at logarithmic growth phase and stationary phase. **c**, The content of NADPH per dry cell weight in *Saccharopolyspora spinosa* at logarithmic growth phase and stationary phase. P value is 0.0033 at logarithmic phase and is 0.0016 at stationary phase. **d**, The content per dry cell weight of NADP+ in *Saccharopolyspora spinosa* at logarithmic growth phase and stationary phase. **e**, The molar ratio of NADPH/NADP+ in *Saccharopolyspora spinosa* at logarithmic growth phase and stationary phase. P value is 0.0003 at logarithmic phase and is 5.5×10^{-5} at stationary phase. All data were represented as mean ± SD (n = 3 independent experiments). Statistical analysis was performed using two-tailed Student's *t*-test.
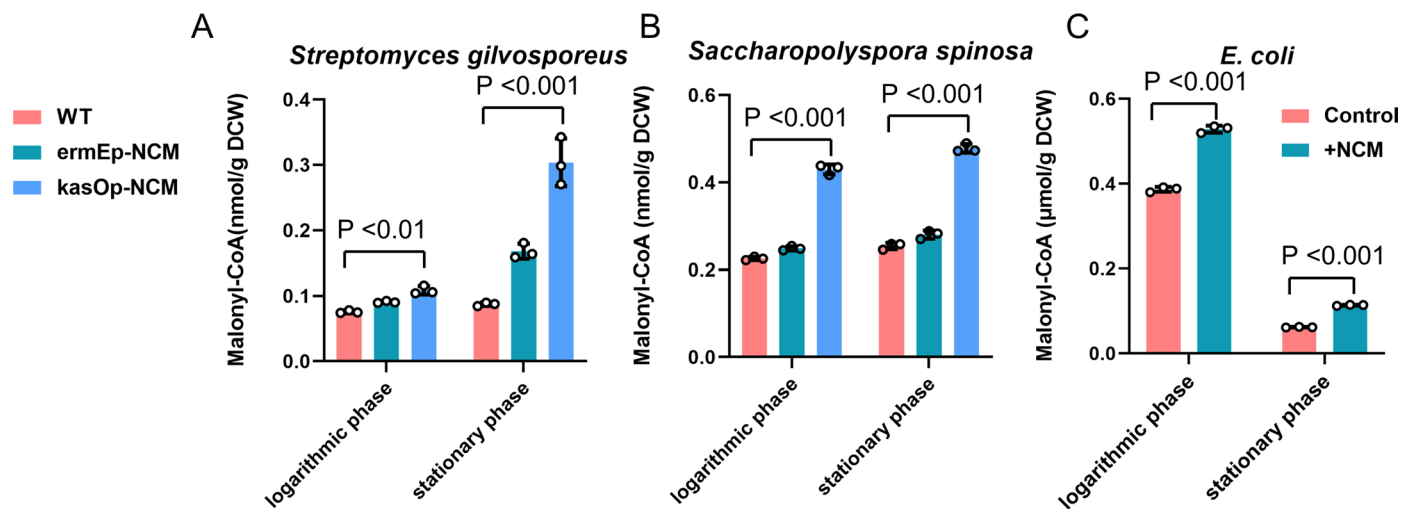
Extended Data Fig. 4 | The intracellular contents of malonyl-CoA in *Streptomyces gilvosporeus, Saccharopolyspora spinosa* and *E. coli*. a, The concentration of malonyl-CoA per dry cell weight in *Streptomyces gilvosporeus* at logarithmic growth phase and stationary phase. P value is 0.0011 at logarithmic phase and is 0.0002 at stationary phase. **b**, The concentration of malonyl-CoA per dry cell weight in *Saccharopolyspora spinosa* at logarithmic growth phase and stationary phase. P value is 7.8×10^{-6} at logarithmic phase and is 6.5×10^{-6} at stationary phase. **c**, The concentration of malonyl-CoA per dry cell weight in *E. coli* at logarithmic growth phase and stationary phase. P value is 1.7×10^{-5} at logarithmic phase and is 3.3×10^{-7} at stationary phase. All data were represented as mean ± SD (n = 3 independent experiments). Statistical analysis was performed using two-tailed Student's *t*-test.
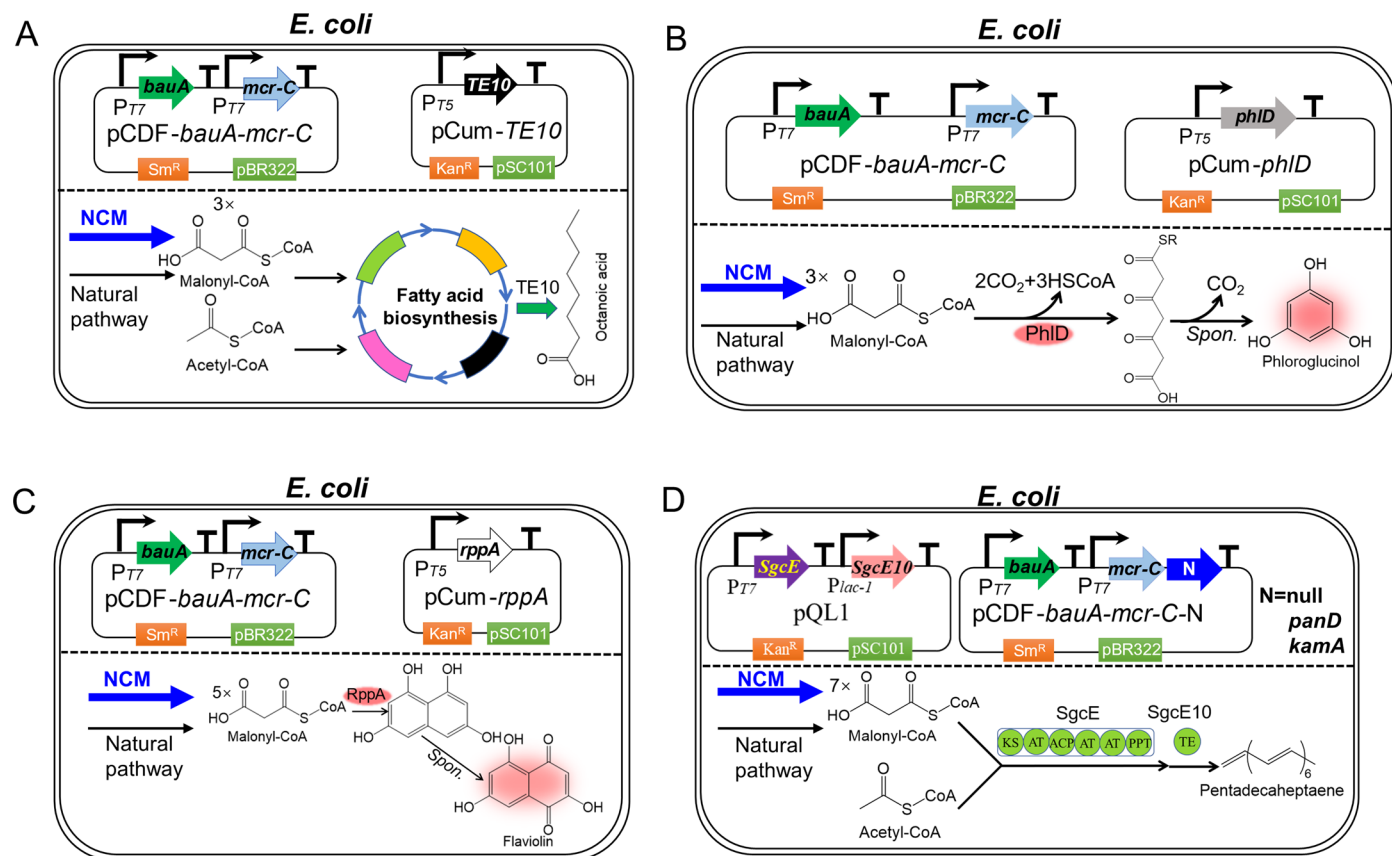
Extended Data Fig. 5 | In vivo production of MDPs in the model microorganism *E. coli*. a, the biosynthetic pathway of octanoic acid in recombinant *E. coli*. **b**, the biosynthetic pathway of phloroglucinol in recombinant *E. coli*. **c**, the biosynthetic pathway of flaviolin in recombinant *E. coli*. **d**, the biosynthetic pathway of pentadecaheptaene in recombinant *E. coli*.
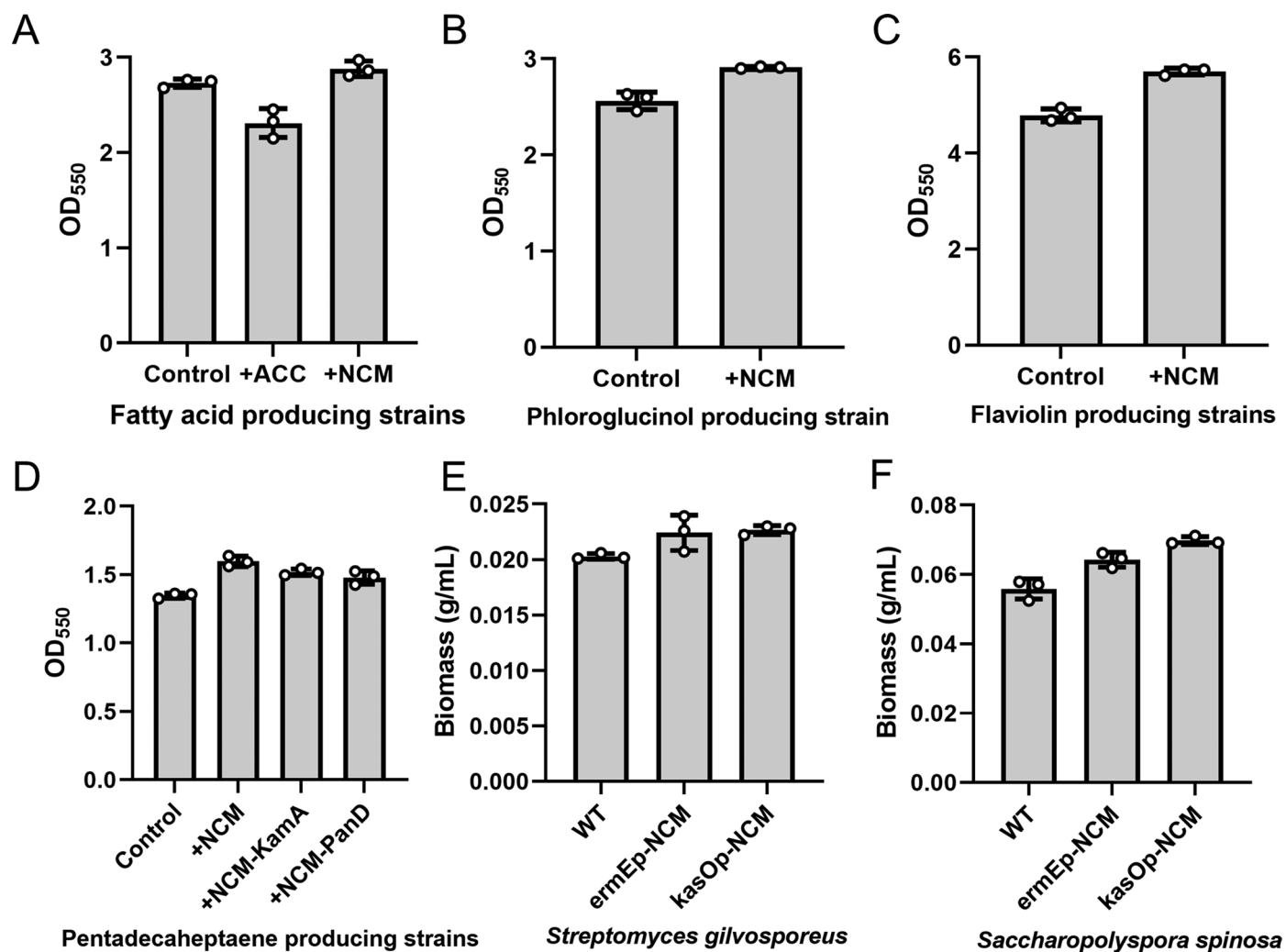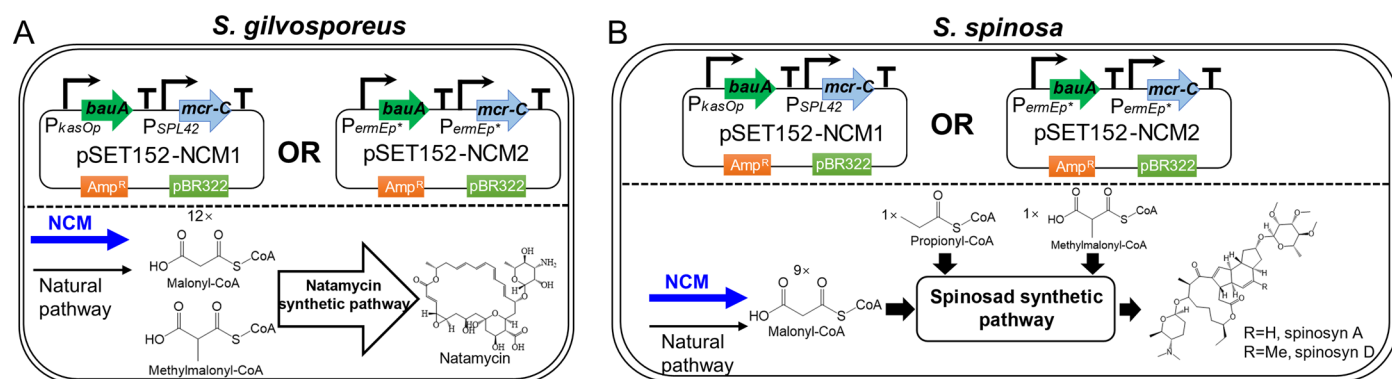
Extended Data Fig. 6 | The biomass of MDPs (malonyl-CoA-derived products) producing strains. a, the final biomass (OD_{550}) of short-chain fatty acid (octanoic acid) producing strains. **b**, the final biomass (OD_{550}) of phloroglucinol producing strains. **c**, the final biomas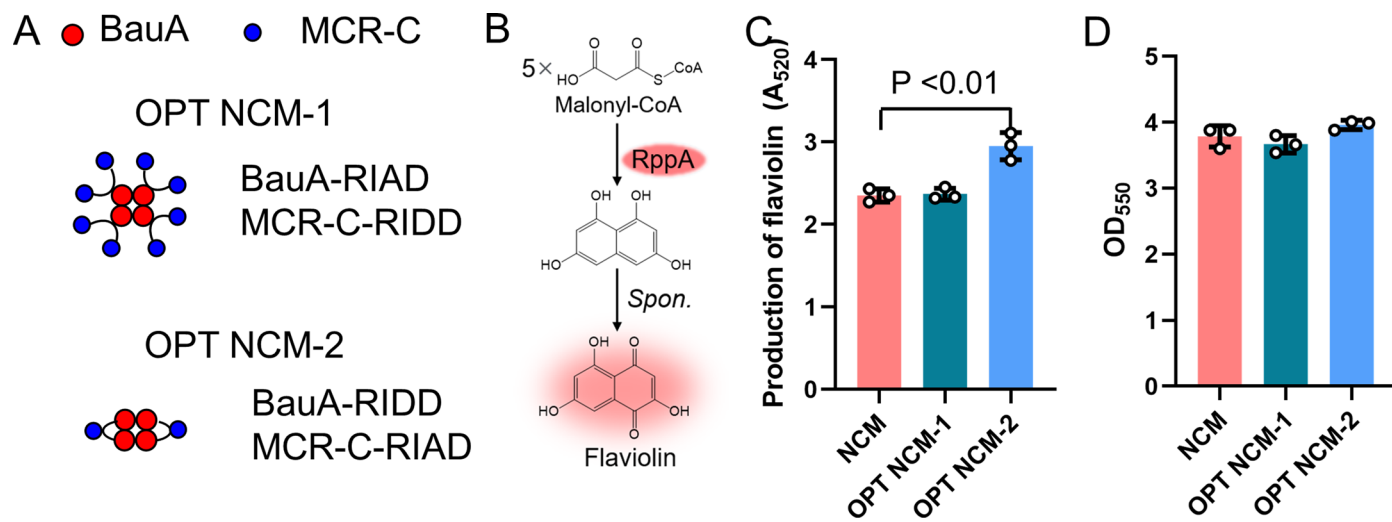s (OD_{550}) of phloroglucinol flaviolin strains. **d**, the final biomass (OD_{550}) of pentadecaheptaene producing strains. **e**, the final biomass (g/mL) of natamycin producing strains. **f**, the final biomass (g/mL) of spinosad producing strains. All data were represented as mean ± SD (n = 3 independent experiments).

Extended Data Fig. 7 | The intracellular contents of β-alanine per dry cell weight in *Streptomyces gilvosporeus* and *Saccharopolyspora spinosa*. a, The content of β-alanine per dry cell weight in *Streptomyces gilvosporeus* at logarithmic growth phase and stationary phase. **b**, The content of β-alanine per dry cell weight in *Saccharopolyspora spinosa* at logarithmic growth phase and stationary phase. All data were represented as mean ± SD (n = 3 independent experiments).

Extended Data Fig. 8 | In vivo production of MDPs in non-model microorganisms. a, the biosynthetic pathway of natamycin in *S. gilvosporeus*. **b**, the biosynthetic pathway of Spinosad in *S. spinosa*.

Extended Data Fig. 9 | Assembly of the NCM pathway enzymes for malonyl-CoA derived flaviolin production. a, the 2 types of assembly optimization. **b**, the malonyl-CoA dependent synthesis of flaviolin. **c**, the flaviolin titers of different strains. P = 0.0048. **d**, the final biomass (OD550) of flaviolin producing strains. All data were represented as mean ± SD (n = 3 independent experiments). Statistical analysis was performed using two-tailed Student's t-test.

nature research

Corresponding author(s):   Chen Yang, Tiangang Liu, Zaigao Tan

Last updated by author(s):   Dec 8, 2023

Reporting Summary

Nature Research wishes to improve the reproducibility of the work that we publish. This form provides structure for consistency and transparency in reporting. For further information on Nature Research policies, see Authors & Referees and the Editorial Policy Checklist.

Statistics

For all statistical analyses, confirm that the following items are present in the figure legend, table legend, main text, or Methods section.

n/a	Confirmed	
☐	☒	The exact sample size (*n*) for each experimental group/condition, given as a discrete number and unit of measurement
☐	☒	A statement on whether measurements were taken from distinct samples or whether the same sample was measured repeatedly
☐	☒	The statistical test(s) used AND whether they are one- or two-sided *Only common tests should be described solely by name; describe more complex techniques in the Methods section.*
☒	☐	A description of all covariates tested
☒	☐	A description of any assumptions or corrections, such as tests of normality and adjustment for multiple comparisons
☐	☒	A full description of the statistical parameters including central tendency (e.g. means) or other basic estimates (e.g. regression coefficient) AND variation (e.g. standard deviation) or associated estimates of uncertainty (e.g. confidence intervals)
☐	☒	For null hypothesis testing, the test statistic (e.g. *F*, *t*, *r*) with confidence intervals, effect sizes, degrees of freedom and *P* value noted *Give P values as exact values whenever suitable.*
☒	☐	For Bayesian analysis, information on the choice of priors and Markov chain Monte Carlo settings
☒	☐	For hierarchical and complex designs, identification of the appropriate level for tests and full reporting of outcomes
☒	☐	Estimates of effect sizes (e.g. Cohen's *d*, Pearson's *r*), indicating how they were calculated

Our web collection on statistics for biologists contains articles on many of the points above.

Software and code

Policy information about availability of computer code

Data collection	Data was collected using: Agilent MassHunter GC/MS Acquisition B.07.05.2479 (GC-FID/MS), BioTek Gen5 v2.09.2 (Plate reader), BLASTp suite (NCBI), Agilent MassHunter Workstation LC/MS Data Acquisition for 6400 Series Triple Quadrupole software (ver. B.08.02)
Data analysis	GC/MS data analysis software: Agilent MassHunter; BioTek Gen5 v2.09.2 (Plate reader)data analysis software: Gen5. 3.08 LC/MS data analysis software: Agilent MassHunter. Compute pI/Mw tool of ExPASy, Microsoft Excel 2021

For manuscripts utilizing custom algorithms or software that are central to the research but not yet described in published literature, software must be made available to editors/reviewers. We strongly encourage code deposition in a community repository (e.g. GitHub). See the Nature Research guidelines for submitting code & software for further information.

Data

Policy information about availability of data

All manuscripts must include a data availability statement. This statement should provide the following information, where applicable:
- Accession codes, unique identifiers, or web links for publicly available datasets
- A list of figures that have associated raw data
- A description of any restrictions on data availability

All the data generated in this study is available within the main text, the Supplementary Information file; source data are provided in the Source Data file. Data is also available from the corresponding author upon request.

Field-specific reporting

Please select the one below that is the best fit for your research. If you are not sure, read the appropriate sections before making your selection.

☒ Life sciences ☐ Behavioural & social sciences ☐ Ecological, evolutionary & environmental sciences

For a reference copy of the document with all sections, see nature.com/documents/nr-reporting-summary-flat.pdf

Life sciences study design

All studies must disclose on these points even when the disclosure is negative.

Sample size	Sample size of at least three was chosen following all previous publications in similar field.
Data exclusions	No data were excluded from the analyses.
Replication	In vitro NCM pathway assays were carried out with five replications. In vitro assays of classic inhibitors/conditions of the natural pathway to NCM pathway were carried out with three replications. The in vivo experiments were repeated with at least three replications to make sure the data reproducibility.
Randomization	All strains for in vivo culture were randomly picked from the LB with antibiotics agar plate.
Blinding	Investigators were not blinded to strains' genotypes during experiments. All in vivo and in vitro data were analysed and checked by multiple authors and reviewed by the corresponding authors.

Reporting for specific materials, systems and methods

We require information from authors about some types of materials, experimental systems and methods used in many studies. Here, indicate whether each material, system or method listed is relevant to your study. If you are not sure if a list item applies to your research, read the appropriate section before selecting a response.

Materials & experimental systems

n/a	Involved in the study
☒	Antibodies
☒	Eukaryotic cell lines
☒	Palaeontology
☒	Animals and other organisms
☒	Human research participants
☒	Clinical data

Methods

n/a	Involved in the study
☒	ChIP-seq
☒	Flow cytometry
☒	MRI-based neuroimaging